



Published in final edited form as:

Cell Rep. 2022 June 21; 39(12): 110958. doi:10.1016/j.celrep.2022.110958.

## Disruption of the lipolysis pathway results in stem cell death through a sterile immunity-like pathway in adult *Drosophila*

Poonam Aggarwal<sup>2,3</sup>, Zilun Liu<sup>1,3</sup>, Guang Qian Cheng<sup>1,3</sup>, Shree Ram Singh<sup>2</sup>, Chunmei Shi<sup>2</sup>, Ying Chen<sup>1</sup>, Ling V. Sun<sup>1,\*</sup>, Steven X. Hou<sup>1,2,4,\*</sup>

<sup>1</sup>State Key Laboratory of Genetic Engineering, School of Life Sciences, Institute of Developmental Biology and Molecular Medicine, Institute of Metabolism and Integrative Biology, Human Phenome Institute, Department of Liver Surgery and Transplantation of Liver Cancer Institute at Zhongshan Hospital, Children's Hospital, Fudan University, Shanghai 200438, China

<sup>2</sup>The Basic Research Laboratory, Center for Cancer Research, National Cancer Institute at Frederick, National Institutes of Health, Frederick, MD 21702, USA

<sup>3</sup>These authors contributed equally

<sup>4</sup>Lead contact

### SUMMARY

We previously showed that the Arf1-mediated lipolysis pathway sustains stem cells and cancer stem cells (CSCs); its ablation resulted in necrosis of stem cells and CSCs, which further triggers a systemic antitumor immune response. Here we show that knocking down Arf1 in intestinal stem cells (ISCs) causes metabolic stress, which promotes the expression and translocation of ISC-produced damage-associated molecular patterns (DAMPs; Pretaporter [Prtp] and calreticulin [Calr]). DAMPs regulate macroglobulin complement-related (Mcr) expression and secretion. The secreted Mcr influences the expression and localization of enterocyte (EC)-produced Draper (Drpr) and LRP1 receptors (pattern recognition receptors [PRRs]) to activate autophagy in ECs for ATP production. The secreted ATP possibly feeds back to kill ISCs by activating inflammasome-like pyroptosis. We identify an evolutionarily conserved pathway that sustains stem cells and CSCs, and its ablation results in an immunogenic cascade that promotes death of stem cells and CSCs as well as antitumor immunity.

### Graphical Abstract

This is an open access article under the CC BY-NC-ND license (<http://creativecommons.org/licenses/by-nc-nd/4.0/>).

\*Correspondence: lingsun@fudan.edu.cn (L.V.S.), stevenhou@fudan.edu.cn (S.X.H.).

#### AUTHOR CONTRIBUTIONS

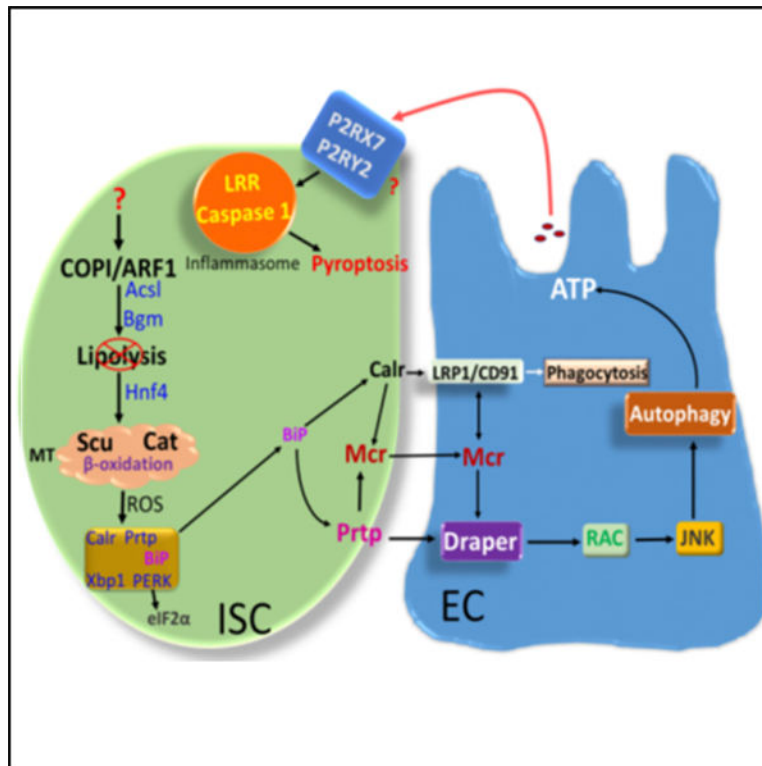
S.X.H., P.A., Z.L., G.Q.C., and L.V.S. conceived and designed the experiments. P.A., Z.L., G.Q.C., S.X.H., C.S., Y.C., and S.R.S. performed the experiments. S.X.H., P.A., Z.L., G.Q.C., and L.S. analyzed the data. S.X.H., P.A., Z.L., G.Q.C., and L.S. wrote the manuscript.

#### SUPPLEMENTAL INFORMATION

Supplemental information can be found online at <https://doi.org/10.1016/j.celrep.2022.110958>.

#### DECLARATION OF INTERESTS

The authors declare no competing interests.



### In brief

Aggarwal et al. show that disruption of Arf1-mediated lipolysis results in stem cell death through a sterile immunity-like pathway in adult *Drosophila*. They identify an evolutionarily conserved pathway that specifically sustains stem cells and cancer stem cells (CSCs), and its ablation results in an immunogenic cascade that promotes death of stem cells and CSCs as well as antitumor immunity.

## INTRODUCTION

The adult *Drosophila* digestive system is an ideal genetic system to study stem cell maintenance. In this system, three organs—the posterior midgut, hindgut, and Malpighian tubules (MTs)—meet and join at the junction of the posterior midgut and hindgut. Intestinal stem cells (ISCs), located in the posterior midgut, divide once every 24 h (Micchelli and Perrimon, 2006; Ohlstein and Spradling, 2006); renal and nephric stem cells (RNSCs), located in the MTs, divide about once a week (Singh et al., 2007; Zeng et al., 2010b, Zeng and Hou, 2011). ISCs and RNSCs can be transformed to produce tumors: ISCs by knocking down their Notch (N) activity, which blocks ISC differentiation and turns on a tumorigenesis cascade (Ohlstein and Spradling, 2006, 2007; Patel et al., 2015), and RNSCs by forcing their expression of a constitutively activated Ras (Zeng et al., 2010b). These transformed stem cells resemble CSCs. N and EGF receptor (EGFR) also regulate apoptosis in progenitor cells (enteroblasts [EBs]) to ensure gut homeostasis in *Drosophila* (Reiff et al., 2019).

Through asymmetric division, ISCs generate new ISCs as well as new EB cells, which, in turn, differentiate into enterocytes (ECs) or enteroendocrine (EE) cells (Micchelli and Perrimon, 2006; Ohlstein and Spradling, 2006). Recent studies demonstrated that ISCs can directly differentiate into EE cells (Zeng et al., 2015; Biteau and Jasper, 2014; Guo and Ohlstein, 2015). N signaling plays a major role in regulating ISC self-renewal and differentiation. The ligand of the N pathway, Delta (DI), is specifically expressed on an ISC and unidirectionally switches on the N signaling pathway in the neighboring EB to promote differentiation of an EB to an EC and inhibit differentiation of an EB to an EE cell (Micchelli and Perrimon, 2006; Ohlstein and Spradling, 2006, 2007).

We found previously that the Arf1-mediated lipolysis pathway is specifically activated in stem cells and sustains stem cells in adult *Drosophila* (Singh et al., 2016). Arf1 is one of the most evolutionarily conserved genes between *Drosophila* and mouse, with an amino acid identity of 95.6% between the two species. We found recently that Arf1-mediated lipid metabolism sustains cancer stem cells (CSCs) and that its ablation triggers immunogenic-like death (immunogenic cell death [ICD]) of CSCs and induces antitumor immunity by exposing damage-associated molecular patterns (DAMPs; calreticulin [Calr], high-mobility group box 1 [HMGB1], and ATP) (Wang et al., 2020).

However, the molecular mechanism that coordinates stem cells/CSCs with neighboring cells to execute the biological processes (stem cell necrosis or anti-tumor immunity) is still unclear. In this study, we dissected the molecular mechanism using the *Drosophila* genetic system. We found that knockdown of the pathway promotes stem cell death through an immunogenic-like and aging cascade. Ablation of Arf1-mediated lipid metabolism in *Drosophila* ISCs resulted in several aging-like hallmarks, including lipid droplet (LD) accumulation, *Reactive oxygen species (ROS)* accumulation, mitochondrial defects, mitophagy activation, and lysosomal protein aggregates, followed by an immunogenic-like cell death (López-Otín et al., 2013; Partridge et al., 2018; Singh et al., 2016; Wang et al., 2020; this study).

ICD is a process that releases DAMPs and activates immune responses to destroy damaged or stressed cells in the absence of microbial components (Garg and Agostinis, 2017; Galluzzi et al., 2017; Rivera Vargas and Apetoh, 2017). These molecules are often present in a given cell compartment and are not expressed or are only somewhat expressed under physiological conditions but strongly induced and then translocated to the cell surface or extracellular space under conditions of stress, damage, or injury. The most important DAMPs are (1) preapoptotic exposure of the ER-sessile molecular chaperone Calr on the cell surface, (2) release of the non-histone nuclear protein HMGB1 into the extracellular space, and (3) active secretion of ATP. With respect to tumors, the surface-exposed Calr facilitates engulfment of tumor-associated antigens by binding to LRP1/CD91 receptors (pattern recognition receptors [PRRs]) on dendritic cells (DCs). During ICD, Calr interacts with another protein, ERp57, and the two are rapidly translocated to the cell surface from the ER lumen before the cells exhibit any sign of apoptosis (Obeid et al., 2007). ERp57 is a disulfide isomerase that has several thioredoxin-like domains and regulates cell redox homeostasis.

We found that knocking down Arf1-mediated lipolysis in ISCs promotes the expression and translocation of ISC-produced DAMPs (Pretaporter [Prtp] and Calr). Like ERp57, Prtp is a disulfide isomerase with several thioredoxin-like domains. The DAMPs may then regulate the expression and secretion of the protein macroglobulin complement-related (Mcr; a complement C5 homolog). The secreted Mcr possibly further controls the expression and localization of EC-produced Draper [Drpr] and LRP1 receptors (PRRs) to activate autophagy in ECs for ATP production. The secreted ATP likely feeds back to kill ISCs by activating inflammasome-like pyroptosis. Therefore, Arf1-mediated lipid metabolism is crucial for stem cell maintenance, and its ablation promotes stem cell decay and anti-tumor immunity through an immunogenic aging cascade.

## RESULTS

### Ablation of the COPI/Arf1-mediated lipolysis pathway selectively kills ISCs

We have demonstrated previously that the COPI/Arf1-lipolysis- $\beta$ -oxidation pathway regulates *Drosophila* ISC survival. Ablation of the pathway results in LD and ROS accumulation, followed by activation of autophagy and stem cell necrosis (Singh et al., 2016). In the previous study, we used an *escargot* (*esg*)-*Gal4*, *UAS-mCD8GFP*; *tub-Gal80<sup>ts</sup>* (*esg<sup>ts</sup>*) driver that depleted Arf1 in ISCs and EBs (*esg<sup>ts</sup>*>*Arf1<sup>RNAi</sup>*; Micchelli and Perrimon, 2006; Singh et al., 2016). To confirm the identity of dying cells, we knocked down *Arf1* by EB-specific Gal4 (*Su(H)GBE-Gal4*, upstream activating sequence [UAS]-GFP; *tub-Gal80<sup>ts</sup>*/UAS-*Arf1<sup>RNAi</sup>*; Zeng et al., 2010a) and ISC-specific Gal4 (*esg-Gal4*, UAS-GFP; *Su(H)GBE-Gal80*, *tub-Gal80<sup>ts</sup>*/UAS-*Arf1<sup>RNAi</sup>*; Wang et al., 2014; Zeng and Hou, 2015). In the ISC-specific Gal4 line, EB expression of *esg-Gal4* is suppressed by *Su(H)GBE-Gal80*, and the combined line only drives gene expression in ISCs. We found that Arf1 knockdown in EBs by EB-Gal4 did not result in cell death (Figures S1A–S1C), and Arf1 knockdown in ISCs by ISC-Gal4 resulted in stem cell death (Figures S1D–S1F). We also generated mosaic analysis with a repressible cell marker (MARCM) clones of FRT<sup>82B</sup>-control, FRT<sup>82B</sup>- $\gamma$ -cop<sup>10</sup>, FRT<sup>82B</sup>-Calr<sup>S062111</sup>- $\gamma$ -cop<sup>10</sup>, and stained DI. We found that the single cell in the  $\gamma$ -cop<sup>10</sup> mutant clone was an ISC that failed to differentiate, and the differentiation defect could be rescued by mutation of a newly identified suppressor Calr (described later) (Figures S1G–S1I'). We further stained Dcp-1 with DI and found that Dcp-1-positive cells were also DI-positive cells in the posterior midgut of *esg<sup>ts</sup>*>*Arf1<sup>RNAi</sup>* flies (Figures S1J and S1K''). We also found no difference in *esg* enhancer trap expression in the remaining ISCs between wild-type and Arf1 knockdown flies, indicating that Arf1 knockdown did not affect *esg* expression (Figures S1L and S1M''').

All of these data suggest that the COPI/Arf1-lipolysis pathway selectively sustains ISC survival. Because the ISC-Gal4 line was generated through combination of several transgenes, it is very difficult to further combine it with more genes as performed in this study; therefore, we used *esg-Gal4* in most experiments. For simplicity, in the following text, we refer to *esg<sup>ts</sup>*>*Arf1<sup>RNAi</sup>* as Arf1 knockdown in ISCs or Arf1-depleted flies.

## Ablation of the COPI/Arf1-mediated lipolysis pathway kills ISCs through a cellular cascade

Mitochondria play an important role from cellular energy metabolism to ROS production. We examined mitochondrial morphology using *UAS-mito-HA-GFP* transgenic flies. In wild-type flies, hemagglutinin (HA) was only weakly expressed in *esg*-expressing cells (Figure 1A; *esg<sup>ts</sup>>mito-HA-GFP*), consistent with previous studies showing that mitochondria of normal ISCs have low respiratory output and sparse cristae (Deng et al., 2018; Koehler et al., 2017). In the Arf1-depleted system (*esg<sup>ts</sup>>Arf1<sup>RNAi</sup>*), HA-marked mitochondria appeared as swollen, broken, and fragmented structures (Figure 1B; *esg<sup>ts</sup>>Arf1<sup>RNAi</sup>+mito-HA-GFP*).

Mitophagy functions to remove damaged or excess mitochondria selectively by the autophagic pathway. We examined the mitophagy activity in *garz*-depleted (*garz* is a guanine nucleotide exchange factor of *Drosophila* Arf1) ISCs and EBs (*esg<sup>ts</sup>* without *UAS-GFP*, *esg<sup>ts</sup>*) using a mitophagy reporter, UAS-mtRosella (Edenharter et al., 2018), with mtRosella consisting of a mitochondrion-targeted dsRed fluorescent protein fused to a pH-sensitive GFP called pHluorin. In normal mitochondria, the green and red signals overlap, whereas in damaged mitochondria, mitophagy transfers the degenerating mitochondria to lysosomal compartments, and the green signal is lost because of the low pH (Rosado et al., 2008). We observed that, in the wild-type *Drosophila* posterior midgut, all mitochondria exhibited green and red overlapping signals (Figures 1C–1C''''; *esg<sup>ts</sup>>mtRosella*). In the *garz*-depleted system (*esg<sup>ts</sup>>garz<sup>RNAi</sup>*), the damaged mitochondria were marked with significantly fewer green but numerous red signals (Figures 1D–1D''''; *esg<sup>ts</sup>>garz<sup>RNAi</sup>+mtRosella*), indicating that damaged mitochondria were incorporated into the lysosomal compartment. Similar to mammalian p62, its *Drosophila* ortholog Ref(2)P is useful for monitoring mitochondrial clearance by mitophagy (Edenharter et al., 2018; Wang et al., 2016). We stained Ref(2)P in *esg>mtRosella* flies (Figures 1C''', 1C'''', 1D''', and 1D''') and found that, in the wild-type *Drosophila* posterior midgut, Ref(2)P was only weakly expressed in mtRosella-marked cells (Figures 1C''' and 1C''''; *esg<sup>ts</sup>>mtRosella*), whereas in the *garz*-depleted posterior midgut, Ref(2)P was very strongly expressed in all mtRosella-marked cells (Figures 1D''' and 1D''''; *esg<sup>ts</sup>>garz<sup>RNAi</sup>+mtRosella*).

These results clearly demonstrated that mitophagy activity was enhanced strongly in the *garz*-depleted system and might have transferred excess damaged mitochondria into lysosomes. The accumulation of p62 suggests that the normal lysosomal capacity was insufficient to process the increased number of damaged mitochondria. We also observed the spread of mitophagy and p62. It has been reported previously that mutations in the *Drosophila* glucosylceramidase beta (GBA) gene resulted in lysosomal accumulation of glucosylceramide and spread of ubiquitinated proteins and *Drosophila* p62/Ref(2)P via extracellular vesicles (EVs) (Jewett et al., 2021; Thomas et al., 2018). It was hypothesized that lysosomal accumulation of glucosylceramide in GBA mutant cells might cause lysosomal stress and influence pathogenic protein aggregate spread via EVs. Similarly, the overloaded lysosomes in *garz*-depleted cells might also have caused lysosomal stress and influence pathogenic protein aggregate spread via EVs.

This information demonstrated that Arf1-ablated ISCs display several aging-like hallmarks (López-Otín et al., 2013; Partridge et al., 2018), from LD accumulation to ROS production,

mitochondrial defect, mitophagy activation, lysosomal protein aggregation, and, finally, stem cell necrosis. Arf1 ablation in ISCs might trigger a stem cell aging and death cascade.

### The Dcp-1 reporter marks necrotic ISCs in the *Drosophila* midgut

We have demonstrated previously that knockdown of Arf1 (Arf79F) promotes stem cell death through necrosis rather than through apoptosis or autophagy-mediated cell death (Singh et al., 2016). To investigate the involvement of different caspases in the cell death process of Arf1-depleted ISCs, we used a Drice-based sensor (DBS) that reports the activity of initiator caspases (mainly Dronc) involved in effector caspase activation in apoptotic cells and a Dcp-1 (Death caspase-1)-based sensor/reporter that specifically reports Dcp-1 activation (Baena-Lopez et al., 2018; L.A. Baena-Lopez, personal communication [described in the STAR Methods]). We observed strong expression of the Dcp-1 reporter, whereas expression of the DBS reporter was unaffected upon knockdown of Arf1 in *esg+* cells (Figures S2A–S2D'). SYTOX green staining confirmed that Arf1 ablation induced necrotic cell death (Figures S2E and S2F). Consistent with our previous report (Singh et al., 2016), overexpression of the apoptotic cell death inhibitors p35 and DIAP1 did not block Arf1 ablation-induced Dcp-1 reporter expression (Figures S2G and S2H'). These results suggest that Dcp-1 is activated in a nonapoptotic and Dronc-independent manner after Arf1 knockdown in *esg+* cells and that the Dcp-1 reporter (sensor) marks necrotic ISCs in the *Drosophila* midgut. This was confirmed by Dcp-1 antibody staining (Figures S1J, S1K'', and 7G–7I'). As described in the STAR Methods, the Dcp-1 reporter possibly marks apoptotic and necrotic cells. In our system, there is only necrotic cell death; therefore, we can use the Dcp-1 reporter as a necrotic cell death marker.

### Identification of new components in the Arf1 ablation-induced stem cell death pathway

To identify the missing links in the Arf1 ablation-induced stem cell aging and death pathway, we conducted a genetic screen to identify genes whose reduction rescued necrotic ISC death in Arf1-depleted flies (*esg-gal4, UAS-GFP, tub-Gal80<sup>s</sup>, UAS-Arf1<sup>RNAi</sup>*) using the Bloomington deficiency kit and deficiencies from other sources. Using this screen, we identified 37 deletions that suppressed the stem cell death phenotypes associated with Arf1 knockdown. After analyzing the candidate genes in these deletions, we selected six genes that may relate to mammalian inflammatory cell death or ICD for further study: *prtp* (CG1837), *Mcr* (CG7586), *Calr* (CG9429), *LRP1* (LDL receptor 1; CG33087), *Dcp-1* (CG5370), and *LRR* (leucine-rich repeat; CG1399). *Calr* is one of the major DAMPs and induces potent anticancer immune responses from dying tumor cells (Garg and Agostinis, 2017; Obeid et al., 2007; Rivera Vargas and Apetoh, 2017). *Prtp* has been identified previously as a ligand for *Drpr* that relocates from the ER to the cell surface of apoptotic cells when they undergo phagocytosis in cell culture (Kuraishi et al., 2009). However, the functions of *Calr* and *Prtp* in cell death and phagocytosis in *Drosophila* are still unclear (Lin et al., 2017; Lu et al., 2017; Timmons et al., 2016). *Mcr* has been shown recently to regulate autophagy cell non-autonomously, with a genetic interaction with *Drpr* during salivary gland cell death and macrophage migration in epithelial wounds (Lin et al., 2017). However, *Mcr* does not directly bind *Drpr*, and the molecular mechanism of its function is still unclear (Lin et al., 2017). *Drosophila* *LRP1* is a homolog of mammalian CD91. During mammalian ICD, the surface-exposed *Calr* binds to CD91/LRP1 antigen-presenting cells (APCs) to promote

phagocytosis of the dying cells (Garg and Agostinis, 2017; Rivera Vargas and Apetoh, 2017). Dcp-1 was described above, and the LRR domain of LRR/CG1399 shows significant homology with that of human NLRC3 (a nucleotide-binding LRR-containing [NLR] protein family member with a caspase activation and recruitment domain 3).

We found that reducing the levels of Dcp-1, LRR, Calr, Prtp, Mcr, and LRP1 using RNAi knockdown or a loss-of-function mutation of the genes in stem cells significantly attenuated the stem cell death phenotypes caused by Arf1 knockdown (Figures 2 and 3), including Dcp-1 reporter expression (Figures 2A–2J and 3K), GFP expression in ISCs and EBs (Figures 3A–3J and 3L), and Ref(2)P expression (Figures 3A–3J and 3M). These data suggest that these six genes function downstream of or in parallel with the Arf1-depletion-induced ISC death pathway.

### Hierarchical relationship among new components in the Arf1 pathway

$\gamma$ -cop and garz are two major components of the COPI/Arf1 complex, which sustains stem cells in *Drosophila* (Singh et al., 2016). We generated MARCM (Lee and Luo, 1999) clones of FRT<sup>82B</sup> control, FRT<sup>82B</sup>- $\gamma$ -cop<sup>10</sup>, and FRT<sup>G13</sup>-garz<sup>211</sup> flies and examined the expression and localization of these new proteins in the posterior midgut (Figures 4, S3O, and S3P). In wild-type control clones of the midgut, these proteins were missing or only weakly expressed (Figures 4A–4E'). In  $\gamma$ -cop<sup>10</sup> and garz<sup>211</sup> mutant clones of the midgut (Figures 4F–4L', S3O, and S3P), we found that (1) expression of phosphorylated eIF2 $\alpha$  (peIF2 $\alpha$ , an ER stress marker), Calr, and Prtp was strongly induced in GFP-marked ISCs (Figures 4F–4H' and S3O), (2) expression of Drpr and LRP1 was induced in ECs (Figures 4K–4L' and S3P), and (3) expression of Mcr was first induced in ISCs on the third day (Figures 4I and 4I') and then diffused to ECs (Figures 4J and 4J').

We also generated FRT<sup>82B</sup>-Calr<sup>S062111</sup> $\gamma$ -cop<sup>10</sup> double mutant MARCM clones (Figures 4M–4R'). In the double-mutant clones, we found that (1) expression of Calr, Mcr, Drpr, and LRP1 was lost, and (2) expression of BiP/GRP78 (another ER stress marker) and Prtp was still strongly induced in GFP-marked ISCs (Figures 4N–4O'). These data suggest that Mcr, Drpr, and LRP1 function downstream of Calr.

We then generated MARCM clones of FRT<sup>82B</sup>- $\gamma$ -cop<sup>10</sup> in different genetic backgrounds and examined the expression and localization of these proteins in the posterior midgut (Figures 5A and S3A–S3N). We found that (1) in MARCM clones of UAS-Prtp<sup>RNAi</sup>; FRT<sup>82B</sup>- $\gamma$ -cop<sup>10</sup> flies, Calr was expressed but Mcr, Drpr, LRP1, and Prtp were not; (2) in MARCM clones of Mcr<sup>EY07421/+</sup>; FRT<sup>82B</sup>- $\gamma$ -cop<sup>10</sup> flies, Calr and Prtp were expressed but Drpr, LRP1, and Mcr were not; (3) in MARCM clones of LRP1<sup>MI03128/+</sup>; FRT<sup>82B</sup>- $\gamma$ -cop<sup>10</sup> flies, Calr and Prtp were expressed and LRP1 and Drpr were not, and expression of Mcr was significantly decreased; and (4) in MARCM clones of Dcp-1<sup>3/+</sup>; FRT<sup>82B</sup>- $\gamma$ -cop<sup>10</sup> flies, Calr, Prtp, Drpr, LRP1, and Mcr were expressed, as observed in MARCM clones of FRT<sup>82B</sup>- $\gamma$ -cop<sup>10</sup> flies.

These data suggest that (1) Calr and Prtp function in parallel downstream of the Arf1-lipolysis pathway, (2) Mcr functions downstream of Calr and Prtp, (3) Mcr and LRP1

regulate each other, (4) Drpr functions downstream of Mcr and LRP1, and (5) Dcp-1 functions downstream of the other five genes (Figure 5B).

### Expression and localization of the new components after ablation of the COPI/Arf1-mediated lipolysis pathway

To investigate how ablation of the COPI/Arf1-mediated lipolysis pathway in ISC affects the downstream proteins, we examined the expression of Calr, Mcr, LRP1, Prtp, Drpr, and BiP in the midgut of wild-type flies and of flies with components of the COPI/Arf1-mediated lipolysis pathway depleted (Singh et al., 2016), including  $\delta$ -cop ( $esg^{ts}>\delta$ -cop<sup>RNAi</sup>), Arf1 ( $esg^{ts}>Arf1^{RNAi}$ ), garz ( $esg^{ts}>garz^{RNAi}$ ), and Acs1 (acyl-coenzyme A [CoA] synthetase long chain;  $esg^{ts}>Acs1^{RNAi}$ ). We found that the downstream proteins were missing or only weakly expressed in the midgut of wild-type control flies (Figures S3Q–S3Z and S4) but induced strongly in the midgut of flies with  $\delta$ -cop-, Arf1-, garz-, or Acs1-depleted ISC systems. In the posterior midgut with gene knockdown of the Arf1 pathway components, Calr and Mcr were co-induced in ISCs, and Mcr was secreted and re-localized to the junctions of ISCs and ECs or junctions between ECs (Figures S3Q–S3V', S5B, S5D, S5G, and S5I). LRP1 was induced in ECs, and some LRP1 was trapped at ISC-EC junctions and colocalized with Calr and Mcr (Figures S3W–S3Z, S5E, and S5J). Prtp and BiP were also co-induced in ISCs (Figures S4A–S4D'', S5A, S5C, S5F, and S5H). Drpr was induced in ECs, moved to the cell surface on the side that was next to a neighboring ISC (compare Figures S4F and S4E), and then was trapped on the ISC surface (Figures S4G and S4H). Mcr colocalized with Prtp and Drpr (Figures S4I–S4L). These data suggest that these proteins coordinately mediate the ISC death process in Arf1-ablated stem cells.

We also examined the expression of Calr, Mcr, LRP1, Prtp, and Drpr in the midgut of flies in which Arf1 was depleted by ISC-Gal4 and found that they were induced just like in  $esg^{ts}Arf1^{RNAi}$  flies (Figures S5K–S5N).

### ER stress functions upstream of DAMPs and PRRs

As described above, two ER stress markers, BiP and peIF2 $\alpha$ , were induced in Arf1-,  $\delta$ -cop-, or  $\gamma$ -cop-depleted flies. Therefore, we next studied the function of ER stress in Arf1 depletion-induced ISC death (Figures S6). We found that knockdown of *Perk*, *Bip*, and *Xbp1* of the ER stress pathway (Hetz and Mollereau, 2014) and feeding flies the ER stress inhibitors sodium 4-phenylbutyrate (PBA) and GSK2606414 significantly rescued ISC death in Arf1-depleted flies (Figures S6A–S6I). peIF2 $\alpha$  was undetectable in the wild-type midgut (Figures S6J–S6J') but induced in the Arf1-depleted ISC system (Figures S6K–S6K'). We also found that feeding flies the ER stress inhibitors PBA and GSK2606414 and knocking down *Perk* inhibited induction of Prtp, Mcr, Calr, LRP1, and Drpr in the Arf1-depleted midgut (Figures S6L–S6R). These data suggested that ER stress functions upstream of DAMPs and PRRs (Figure 5B).

### Arf1 ablation kills stem cells through inflammasome-like pyroptosis

Our previous report (Singh et al., 2016) and data suggested that knockdown of the Arf1-mediated lipolysis pathway in ISCs kills the cells through necrosis. There are two forms of regulated or programmed necrosis: necroptosis and pyroptosis (reviewed in Wallach

et al., 2016; Yuan et al., 2016). Because necroptosis is poorly conserved in the animal kingdom (Dondelinger et al., 2016), we investigated the function of pyroptosis in Arf1 ablation-induced stem cell death.

*Drosophila* Dcp-1 is the homolog of mammalian caspase-1. As described above, the Dcp-1 reporter was induced strongly in Arf1-ablated ISCs. We also found that Dcp-1 protein was induced after Arf1 knockdown (compare Figures 7H and 7H' with 7G and 7G'). These data suggest that Dcp-1 is activated in necrotic stem cells after Arf1 knockdown and may mediate pyroptosis like mammalian caspase-1. To better understand the conservation of the pyroptosis pathways in *Drosophila*, we performed a BLAST search to identify the *Drosophila* homologs of ASC (apoptosis-associated speck-like protein containing a caspase activation and recruitment domain-CARD; an adapter protein), GSDMD (Gasdermin-D), and the NLR protein family. We found no homologs of ASC and GSDMD in *Drosophila*, but the identified LRR domain of LRR protein has a significant homology with that of the human NLRC3 LRR domain that also presents in some innate immune receptors that respond to DAMP and PAMP signals (Garg and Agostinis, 2017; Obeid et al., 2007; Rivera Vargas and Apetoh, 2017). Therefore, inflammasome pyroptosis maybe only partially conserved between *Drosophila* and mammals. As described above, reducing the amount of Dcp-1 or LRR significantly attenuated ISC death caused by Arf1 knockdown (Figures 2 and 3).

We demonstrated previously that Arf1 inhibitors markedly reduce MT stem cell tumors in *Drosophila* by inhibiting the lipolysis pathway (Singh et al., 2016). Knocking down N activity blocks ISC differentiation and promotes ISC tumors (Ohlstein and Spradling, 2006, 2007; Patel et al., 2015). We tested the effect of inflammasome and autophagy inhibitors along with the Arf1 inhibitor Golgicide A (GCA) on midgut and MT stem cell tumors in *Drosophila* (Figures 6A–6K and S7A–S7J). Caspase-1 activation and inflammasome assembly require K<sup>+</sup> efflux, which is facilitated by ATP-mediated P2×7 receptor activation. Because these inhibitors have not been biochemically tested for inhibiting the *Drosophila* proteins, we blocked each function with several different inhibitors. We first blocked ATP function by inhibiting pannexin-1-mediated release of ATP with carbenoxolone (CBX) and DIDS (disodium 4,4'-diisothiocyanatostilbene-2,2'-disulfonate) or inhibiting the P2×7 pathway using oxidized ATP (an antagonist of the P2×7 receptor, Derangère et al., 2014). We then blocked ATP receptors with suramin (a nontoxic broad-spectrum inhibitor of purinergic receptors) and PPAD (pyridoxalphosphate-6-azophenyl-2',4'-disulfonic acid; a broad-spectrum antagonists of P2X and P2Y purinergic receptors). We also used the type 2 diabetes drug glyburide, which has been reported to prevent inflammasome activation (Lamkanfi et al., 2009), and an autophagy inhibitor, Bafilomycin, to block autophagy activation in Arf1-deficient stem cell tumors. We found that all of these inhibitors of inflammasome and autophagy dramatically blocked GCA-induced cell death of stem cell tumors in both systems (Figures 6A–6K and S7A–S7J). The pores on the plasma membrane (membrane rupture) and propidium iodide (PI) staining are two other features of pyroptosis (Wallach et al., 2016). In our previous publication (Singh et al., 2016), the membrane rupture phenotype was only detected in Arf1-depleted but not wild-type ISCs, and the PI signal was only observed in the Arf1-depleted but not wild-type ISCs. These data suggest

that an inflammasome-like pathway may mediate ISC pyroptosis in Arf1-depleted flies. Arf1 ablation kills stem cells through ATP induced inflammasome-like pyroptosis

We then examined the ATP expression using an ATP transgenic reporter (Tsuyama et al., 2013; UAS-AT1.NL; Figure S7K) in the ISC system and ECs (Figures 7A–7C and 7F). We found that the reporter was only weakly expressed in the wild-type posterior midgut (Figures 7A and 7F; *esg.NP<sup>ts</sup>>AT1.NL*) but strongly induced in ECs after Arf1 knockdown (Figures 7B and 7F; *esg.NP<sup>ts</sup>>Arf1<sup>RNAi</sup>+AT1.NL*), whereas a defective reporter, UAS-AT1.RK, which does not bind ATP, was not induced in ECs after Arf1 knockdown (Figures 7C and 7F; *esg.NP<sup>ts</sup>>Arf1<sup>RNAi</sup>+AT1.RK*). Expression of the ATP reporter was also strongly induced after feeding flies the Arf1 inhibitor GCA (Figures 7D and 7F) but not GCA + Bafilomycin (Figures 7E and 7F), indicating that autophagy may function upstream of ATP induction. These results indicated that knocking down Arf1 in ISCs may induce ATP in ECs, which could activate the inflammasomes in ISCs in a feedback manner (Figure 7K).

Decreasing the expression of the genes *Atg13*, *Drpr*, and *LRP1* by half in Arf1-depleted flies rescued ISC death and dramatically blocked Dcp-1 expression (Figures 7G–7J and S7L–S7N), suggesting that Dcp-1 functions downstream of these genes. Knockdown of Arf1 and *Acs1* in ISCs induced strong *Drpr* expression and autophagy in ECs (Figures S7O–S7W). Knockdown of Dcp-1 or LRR in ISCs and the decrease in *Atg14* expression by half in Arf1-depleted flies rescued ISC death but did not change the expression of *Drpr* in ECs (Figures S7O–S7W), suggesting that autophagy, Dcp-1, and LRR may function downstream of *Drpr*. Decreasing the expression of Dcp-1 and LRR by half in Arf1-depleted flies rescued ISC death but did not change autophagy in ECs (Figures S7V and S7W), suggesting that Dcp-1 and LRR function downstream of autophagy. *Drpr*, *LRP1*, and autophagy are functional in ECs (Singh et al., 2016; this study). These findings suggest that knockdown of Arf1-mediated lipolysis in ISCs may first activate the *LRP1*-*Drpr*-autophagy pathway in ECs to promote ATP production. The secreted ATP may then activate inflammasomes in ISCs in a feedback mechanism to kill the stem cells through pyroptosis (Figure 7K).

## DISCUSSION

Stem cells are “root” cells in an organism. Their functional decay or decline may be one of the important causes of organismal aging and disease. In this study, we demonstrated that Arf1-mediated lipid metabolism sustains stem cells and that its ablation triggers an immunogenic-like stem cell death cascade. The dying stem cells display the following features: LD accumulation, mitochondrial defects, ROS production, ER stress and release of DAMPs to activate PRRs in neighboring ECs, mitophagy activation, lysosomal protein aggregations, and ISC necrosis through inflammasome-like pyroptosis (Singh et al., 2016; Figure 7K). These features are similar to hallmarks of aging (López-Otín et al., 2013; Partridge et al., 2018). Arf1 ablation in ISCs might trigger a stem cell aging and death cascade.

The gold standard method for evaluating ICD is *in vivo* tumor vaccination. We previously performed an experiment of vaccination in Arf1-ablated mice (Wang et al., 2020). In this study, we demonstrated that many of the factors that contribute to ICD are expressed

and function in Arf1-ablated flies, indicating that the pathway is partially conserved between *Drosophila* and mammals. However, it is important to confirm conserved biological functions of the ICD in *Drosophila* in future experiments. Similarly, inflammasome pyroptosis is only partially conserved between *Drosophila* and mammals. It is important to confirm the pathway by using inflammasome markers and demonstrate conserved biological functions of the pathway in *Drosophila* in future experiments.

A previous report demonstrated that Mcr, through Drpr, cell non-autonomously regulates autophagy during wound healing and salivary gland cell death in *Drosophila* and that Prtp is not involved in this Mcr-Drpr-mediated autophagy induction (Lin et al., 2017). Mcr is an analog of mammalian C1q/C5 (Flybase; Lin et al., 2017). C1q binds to the Calr-LRP1 coreceptor in mammals (Byrne et al., 2013; Sim et al., 1998), and Mcr binds to LRP1 (Flybase) in *Drosophila*. In this study, we found that Calr and Prtp function in parallel or downstream of the Arf1-lipolysis pathway and regulate the expression of Mcr and LRP1. Mcr and LRP1 further regulate each other and control the expression of Drpr. Calr and Prtp also regulate the expression of their respective receptors, LRP1 and Drpr. This information suggests that two interconnected complexes, Calr-Mcr-LRP1 and Prtp-Drpr, function downstream of the Arf1-lipolysis pathway and coordinately regulate ISC death.

### Immunogenic/coordinated cell death

In the mammalian immune system, DCs are activated after DAMPs bind to PRRs on their surface. The activated DCs present antigens to T cells, and the activated T cells kill damaged cells (Abbas et al., 2018). In this study, we found that ablation of the COPI/Arf1-mediated lipolysis- $\beta$ -oxidation pathway in stem cells induced expression of DAMPs, which then activate the phagocytic ECs through PRRs (LRP1 and Drpr) on the ECs to kill the stem cells. These findings suggest that such a coordinated cell death process is not limited to mammalian immune responses. In another naturally occurring example, Drpr pathway phagocytosis genes in follicle cells (FCs) non-autonomously promote nurse cell (NC) death in the developing *Drosophila* ovary (Timmons et al., 2016). Although it is not clear how the stretch FCs time the precise developmental death of NCs, in light of our present findings, it is possible that a metabolic or stress signal during this developmental stage increases DAMPs in NCs to activate the Drpr pathway in FCs and non-autonomously promote NC death. DAMPs are also induced in organs during organ transplantation as a result of ischemic damage from the interrupted blood supply while the organ is outside of the body. The DAMPs induced in a graft stimulate immune responses mediated by host innate cells at the site of the graft and the donor's innate immune system and contribute to graft rejection (Abbas et al., 2018). Drpr-mediated phagocytosis is also an essential process during development and in maintenance of tissue homeostasis in several systems (Li and Baker, 2007; MacDonald et al., 2006; Zhou et al., 2001). As mentioned above, the Mcr-Drpr pathway is involved in autophagy induction during wound healing and salivary gland cell death in *Drosophila* (Lin et al., 2017). We propose that such a coordinated cell death (CCD) is a novel and general cell death process in which death of abnormal or altered cells occurs by first sending danger signals (such as DAMPs) and then activating neighboring cells to execute the death process. The abnormality or alteration can be metabolic stress (such as disruption of Arf1-mediated lipid metabolism in stem cells), developmental changes (such

as NC death during *Drosophila* ovary development or salivary gland cell death during metamorphosis), or damage during wound healing or circulation blockage during ischemic damage or pathogen infection. The danger signals then activate phagocytes and other cells (such as T cells) to cell non-autonomously promote targeted cell death. CCD may mediate cell aging/death and organ degeneration under physiological conditions or CSC death and anti-tumor immunity under pathological conditions.

Our finding that the DAMP-Mcr-LRP1/Drpr pathway connects metabolically stressed stem cells after Arf1 ablation to activation of phagocytic ECs to kill the stem cells will enable us to further dissect the CCD mechanism in *Drosophila*. Arf1 is one of the most evolutionarily conserved genes, and the DAMP-Mcr/C1q-LRP1/Drpr pathway is well conserved throughout evolution. CCD involves coordination or communication of two or more different cells. Model organisms such as *Drosophila*, with their advanced genetic tractability and well-characterized cellular histology, will serve as valuable *in vivo* models for dissecting the detailed cellular and molecular mechanisms of CCD. These findings may lead to new therapeutic strategies for many human diseases, such as induction of anti-tumor immunity in individuals with cancer and the blocking of neuronal death in individuals with neurodegenerative conditions.

### Limitations of the study

In this study, we identified an evolutionarily conserved pathway that sustains stem cells, and its ablation results in an ICD cascade that promotes death of stem cells through inflammasome-like pyroptosis. We demonstrated that many of the factors that contribute to ICD and inflammasome-like pyroptosis are expressed and function in Arf1-ablated flies. However, the gold standard method for evaluating ICD is *in vivo* tumor vaccination. The components of ICD and inflammasome-like pyroptosis are only partially conserved between *Drosophila* and mammals. It is important to further confirm the pathway by using inflammasome markers and demonstrate conserved biological functions of the pathway in *Drosophila* in future experiments.

## STAR★METHODS

### RESOURCE AVAILABILITY

**Lead contact**—Further information and requests for resources should be directed to and will be fulfilled by the lead contact, Steven X. Hou (stevenhou@fudan.edu.cn).

**Materials availability**—All unique reagents generated in this study are available upon request.

### Data and code availability

- All data reported in this paper will be shared by the lead contact upon request.
- This paper does not report original code.
- Any additional information required to reanalyze the data reported in this paper is available from the lead contact upon request.

## EXPERIMENTAL MODEL AND SUBJECT DETAILS

**Fly strains**—*NPI-Gal4* (from DGRC), *esg-Gal4* (from Shigeo Hayashi), *Drpr*<sup>5</sup> (from Marc Freeman), *3XCh-atg8a*—the autophagosome marker *Atg8a* tagged with mCherry (ChAtg8a) under the control of its endogenous promoter (from Gabor Juhasz), *Atg13*<sup>81</sup> and *Atg14*<sup>5.2</sup> (from Tor Erik Rusten), *LRR*<sup>UM-8319-3</sup> (from Kyoto Stock Center), *prtp*<sup>1</sup> and *prtp*<sup>2</sup> (from Yoshinobu Nakanishi), *garz*<sup>211</sup> (from Stefan Luschnig, Wang et al., 2012) were recombined onto the FRT<sup>G13</sup> chromosome, *UAS-mtRosella* was obtained from Juan Navarro (Edenharter et al., 2018) and *UAS-ATI.NL* and *UAS-ATI.RK* were from Tadashi Uemura (Tsuyama et al., 2013).

The following fly strains were obtained from the Bloomington Drosophila Stock Center (BDSC) at Indiana University: *LRR*<sup>RNAi</sup>—BL41686 (TRiP ID HMS02250), whose phenotypes were confirmed by another independent RNAi line (NIG stock ID 1399R-1), *Dcp-1*<sup>Prev1</sup> and *Dcp-1*<sup>3</sup>, *Dcp-1*<sup>RNAi</sup>—BL38315 (TRiP ID HMS01779), *Prtp*<sup>RNAi</sup>—BL56965 (TRiP ID HMC04406), *Calr*<sup>S114307</sup>—BL4545, FRT<sup>82B</sup>—*Calr*<sup>S062111</sup>—BL37724, *Xbp1*<sup>RNAi-1</sup>—BL25990, *Xbp1*<sup>RNAi-2</sup>—BL36755, *Mcr*<sup>RNAi</sup>—BL65896, *BiP*<sup>RNAi</sup>—BL32402, *LRP*<sup>EY07878</sup>—BL16864, *LRP*<sup>MI03128</sup>—BL58610, *Perk*<sup>RNAi</sup>—BL35162, *Mcr*<sup>EY07421</sup>—BL15997, mito-HA-GFP—BL8442, FRT<sup>52B</sup>-*UAS-Ras*<sup>V12</sup>, FRT<sup>52B</sup>-*UAS-N<sup>DN</sup>*, *hs-flp.UAS-Src-EGFP*; FRT<sup>52B</sup>(*wt*).*UAS-EGFP (PMML)*, FRT<sup>G13</sup>-*garz*<sup>211</sup> *tub-Gal80<sup>s</sup>*, FRT<sup>82B</sup>-*tub-Gal80*, *hs-flp*<sup>12</sup> and FRT<sup>82B</sup>- $\gamma$ -cop<sup>10</sup>, FRT<sup>82B</sup>-*Calr*<sup>S062111</sup>,  $\gamma$ COP<sup>10</sup> was constructed in our laboratory. *Arf1*<sup>RNAi</sup>-VDRC Transformant ID 23082 (v23082), in which the *Arf1* RNA level was reduced to 39.0% in the *Act-Gal4/UAS-Arf1*<sup>RNAi</sup> flies (Zeng et al., 2015), whose phenotypes were confirmed by two independent RNAi lines (v103572 and v23080),  $\delta$ -cop<sup>RNAi</sup>-v41551 {the  $\delta$ -cop RNA level was reduced to 14.3% in *Act-Gal4/UAS- $\delta$ -cop*<sup>RNAi</sup> flies [Zeng et al., 2015], and the phenotypes were confirmed by an independent RNAi line [Bloomington stock number 31764 (BL31764 (TRiP ID HM04076))], *garz*<sup>RNAi</sup>-VDRC Transformant ID 42141 (v42141), whose phenotypes were confirmed by another independent RNAi line—BL31232 [(TRiP ID JF01013), the *garz* RNA level was reduced to 52.4% in the *Act-Gal4/UAS-garz*<sup>RNAi</sup> (BL31232) flies (Zeng et al., 2015)]; and *Acs1*-BL27729 [(TRiP ID JF02811), in which the *Acs1* RNA level was reduced to 25.5% in the *Act-Gal4/UAS-Acs1*<sup>RNAi</sup> flies (Zeng et al., 2015)]. The sequences used for each VDRC knock-down strain are available at <https://stockcenter.vdrc.at>) and for each Bloomington knock-down strain at <http://flystocks.bio.indiana.edu>.

w; 10XSTAT92E-GFP (transcriptional reporters of JAK/STAT activity) marks both ISC and EB in posterior midgut (Beebe et al., 2010) was obtained from Dr. Baeg (Ayala-Camargo et al., 2007).

*Su(H)GBE-Gal4* was generated in our laboratory (Zeng et al., 2010). *esg-Gal4.UAS-GFP;tub-Gal80ts.Su(H)GBE-Gal40 (Isc-Gal4)* was generated in our laboratory (Wang et al., 2014; Zeng et al., 2015). In brief, the EB expression of *esg-Gal4* was suppressed by *Su(H)GBE-Gal40* and therefore the combined line only drives gene expression in ISCs.

**DBS and Dcp-1 reporters**—The DBS reporter was previously reported (Baena-Lopez et al., 2018). In brief, Drice is fully activated by two sequential steps of enzymatic processing,

with the first cleavage step being mediated by initiator caspases (mainly by Dronc). Upon this first cleavage, Drice is split into two subunits (large and short), which remain strongly associated to form the active protease. Luis Alberto Baena-Lopez's group capitalized on this processing step to devise a reporter of initiator caspase activation, which was hereafter referred to as the Drice-based sensor (DBS). They created one version of DBS that only retained 16 amino acids downstream of the Dronc cleavage site (DBS-S). Their results suggest that DBS-S is able to report on caspase activation in apoptotic cells, and there is no inadvertent or nonspecific cleavage of the DBS-S template without apoptotic stimuli. Similarly, they created another reporter based on Dcp-1 cleavage and activation (Alberto, unpublished). "The signal coming from this line is broader than the obtained with DBS and not always fully overlap with DBS. There are potentially different ways to interpret these results and the referees of our paper decided to ask us to remove this information, so this line is unpublished. However, I will be happy to share it with you if you think that you can do a good use of it." (Steven Hou's personal communication with Alberto).

We obtained these two reporter lines from Alberto. Interestingly, we observed strong expression of Dcp-1 reporter while the expression of DBS sensor was unaffected upon knocking down of Arf1 in the *esg*<sup>+</sup> cells (Figure S4). As described in our previous publication (Singh et al., 2016) and this study, knockdown of Arf1 (Arf79F) promotes stem cell death through necrosis rather than through apoptosis or autophagy-mediated cell death. The Dcp-1 reporter possibly marks both apoptotic and necrotic cells (as Alberto said above: "the signal coming from this line is broader than the obtained with DBS and not always fully overlap with DBS"). In our system, there is only necrotic cell death, therefore we can use it as a necrotic cell death marker. A previous study already showed the non-apoptotic role of Dcp-1 in Dronc independent manner (Shinoda et al., 2019).

## METHOD DETAILS

**Suppressor screen**—To identify the missing links in the Arf1-ablation-induced stem cell aging and death pathway, we conducted a genetic screen to identify genes that reduced expression of which rescued necrotic ISC death in the Arf1-depleted flies (*esg-gal4*, UAS-GFP; *tub-Gal80ts*, UAS-Arf1RNAi). Overall, we conducted 3 rounds screen to nail down the involved genes. The screen was initially performed by using 474 deletions in the Bloomington deficiency kit. Because most of the deficiencies are homozygous lethal, adult progenies with deficiency-Arf1-depleted heterozygotes (*Df*/Arf1RNAi) were transferred to new vials at 29°C for 5 days before dissection. We collected the intestines of 15 female flies in both the control and experimental groups, and the total number of GFP-positive cells per unit area was further counted.

29 positive deletions were further narrowed down by using 175 additional deletions from Bloomington and other sources. 37 deletions out of the above 175 could suppress cell death caused by Arf1 ablation. The 183 mapped genes from these 37 deficiency strains were further used for screening through testing mutants or RNAis of the candidate genes within the deletion regions. After analysis of the current knowledge of these genes, we selected six genes that may relate to the mammalian inflammatory or immunogenic cell death for further study: *prtp* (CG1837), *Mcr* (CG7586), *Calr* (CG9429), *LRP1* (LDL receptor 1

(CG33087), Dcp-1 (CG5370), LRR (leucine-rich repeat, CG1399). Each of these six genes was confirmed by more than 3 different RNAi lines or traditional mutants. Details of the deficiency information are available at the Bloomington web page <https://bdsc.indiana.edu/>.

The screening data supporting this study have not been deposited in a public repository because the experiments are still undergoing, but are available from the corresponding author on request.

**PMML clone assay**—GFP-labeled midgut and renal nephric stem cell (RNSC) tumor clusters were induced by expressing  $N^{DN}$  in midgut and  $Ras^{V12}$  in RNSC clones, using the positively marked mosaic lineage (PMML) labeling technique (Kirilly et al., 2005; Zeng et al., 2010b) in adult *Drosophila*. The flies with  $N^{DN}$ -PMML and  $Ras^{V12}$ -PMML clones were cultured for 4 days at room temperature on normal food to allow tumor growth and then switched to food with the indicated drugs for another 4 days. We classified the tumors into five categories based on the total number of GFP-positive cells in each tumor clone (<10 cells, 10–20 cells, 20–50 cells, 50–100 cells and >100 cells).

**MARCM clone assay**—To induce MARCM clones, three- or four-day-old adult female flies were heat-shocked three times with an interval of 8–12 h, at 37°C, for 45 min. The flies were transferred to daily fresh food after the final heat shock, and their posterior midgut was processed for staining at the indicated times.

**RNAi-mediated gene depletion**—Four male *UAS-RNAi* transgenic flies were crossed with 8 female virgins of *esg<sup>ts</sup>* (*esg-Gal4*, *UAS-GFP*; *tub-Gal80<sup>ts</sup>*) at 18°C. Adult progenies with the desired genotype were transferred to new vials at 29°C for the indicated times before dissection.

**Histology and image capture**—Fly intestines were dissected in PBS and fixed in PBS containing 4% formaldehyde for 30 min. After three 5-min rinses with PBT (PBS +0.1% Triton X-100), the samples were blocked in PBT containing 5% normal goat serum overnight at 4°C, and then incubated first with the primary antibody at room temperature for 2 h, and next with a fluorescence-conjugated secondary antibody for 1 h at room temperature. Samples were mounted in Vectashield mounting medium with DAPI (Vector Laboratories).

The following antibodies were used: rabbit polyclonal anti-BiP (1:200; Novus Biologicals, Cat # NBP1–06274); guinea pig polyclonal anti-Mcr (1:200; from Robert Ward); rabbit polyclonal anti-Calr (1:1000; Abcam, Cat # ab2907); rabbit polyclonal anti-LRP1 (1:1000; from Suzanne Eaton); mouse monoclonal anti-Drpr (1:100; DSHB 8A1); mouse monoclonal anti-Prtp (1:100; generated in our laboratory); rabbit polyclonal anti-peIF2 $\alpha$  (1:1000; Cell Signaling, Cat # 9721S); rabbit polyclonal anti-Ref2P (Abcam, Cat # ab178440); rabbit polyclonal anti-HA tag (Cat # ab9110); rabbit polyclonal anti-GFP (1:500, Thermo Fischer Scientific, Cat # A6455); and mouse monoclonal anti-GFP (1:100; Thermo Fischer Scientific, Cat# A11120). Secondary antibodies were goat anti-mouse, anti-guinea pig; and goat anti-rabbit IgG conjugated to Alexa 488 or Alexa 568 (1:400; Thermo Fischer Scientific). Images were captured with the Zeiss LSM 510, 710 and 780 confocal

microscopy, and processed with LSM Image Browser, ZEN blue, and ImageJ software. One representative image from n flies tested in a single experiment was shown. Experiments were repeated three times.

**FRET imaging and analysis**—The FRET-based ATP biosensors, ATeams, were described in Tsuyama et al. (2013). ATeam BioSensor conformation changes from open to closed after binding to ATP, and this conformation change can enhance FRET from CFP (msecFP) to TFP (cp173-mVenus). We selectively expressed AT1.03NL in ISCs and EBs by using *esg.NP1*ts drivers. For FRET imaging, the adult flies were kept at 29°C, the temperature at which the probe is optimized to detect changes in physiologically relevant ATP levels. After four days of treatment at 29°C, the flies' intestines were dissected and placed in PBS for detection. Finally, the fluorescence emission ratios of AT1.03NL was measured by LSM 710 confocal microscope to obtain the concentration of ATP.

## QUANTIFICATION AND STATISTICAL ANALYSIS

To determine the percentage of GFP<sup>+</sup>, Dcp-1<sup>+</sup> and Ref(2)P<sup>+</sup> cells, the cells were counted with respect to the total number of cells in a 5000- $\mu\text{m}^2$  area of a single confocal plane. In *esg<sup>Δ8</sup>* samples, cells were counted in the posterior midgut. Cells per tumor were determined by counting the total number of nuclei within GFP<sup>+</sup> tumors and the tumor size was calculated by measuring the GFP<sup>+</sup> area in a fixed 5000- $\mu\text{m}^2$  area of a single confocal plane.

All the images were taken with the LSM780 confocal using the similar settings (Zeiss). Data are presented as mean + standard error mean (s.e.m). Sample sizes (N) reported reflect the number of individual guts. Statistical analysis was performed using two-tailed Student's t-test. p values were interpreted as p < 0.001 as \*\* and p < 0.0001 as \*\*\* respectively considered as statistically significant.

## Supplementary Material

Refer to Web version on PubMed Central for supplementary material.

## ACKNOWLEDGMENTS

We thank Luis Alberto Baena-Lopez for providing DBS and Dcp-1 reporters. We also thank Gabor Juhasz, Tor Erik Rusten, Yoshinobu Nakanishi, Stefan Luschig, Juan Navarro, Tadashi Uemura, Shigeo Hayashi, Marc Freeman, VDRC, and the Kyoto and Bloomington Stock Centers for fly stocks; Robert Ward, Suzanne Eaton, and the Developmental Studies Hybridoma Bank for antibodies; and S. Lockett for help with the confocal microscope. This research was supported by the National Natural Science Foundation of China (NSFC; 92057205 and 32150710518 to S.X.H.), the National Key Research and Development Program of China (2019YFA0802303 to L.S.), and the Intramural Research Program of the National Institutes of Health.

## REFERENCES

- Abbas AK, Lichtman AH, and Pillai S (2018). Innate immunity. In Cellular and Molecular Immunology, Abbas AK, Lichtman AH, and Pillai S, eds. (ELSEVIER), pp. 57–95.
- Ayala-Camargo A, Ekas LA, Flaherty MS, Baeg GH, and Bach EA (2007). The Jak/stat pathway regulates proximo-distal patterning in drosophila. *Dev. Dynam* 236, 2721. 10.1002/dvdy.21348.
- Baena-Lopez LA, Arthurton L, Bischoff M, Vincent JP, Alexandre C, and McGregor R (2018). Novel initiator caspase reporters uncover previously unknown features of caspase-activating cells. *Development* 145, 23.

- Beebe K, Lee WC, and Micchelli CA (2010). JAK/STAT signaling coordinates stem cell proliferation and multilineage differentiation in the *Drosophila* intestinal stem cell lineage. *Dev. Biol* 338, 28–37. [PubMed: 19896937]
- Biteau B, and Jasper H (2014). Slit/Robo signaling regulates cell fate decisions in the intestinal stem cell lineage of *Drosophila*. *Cell Rep* 7, 1867–1875. 10.1016/j.celrep.2014.05.024. [PubMed: 24931602]
- Byrne JC, Ní Gabhann J, Stacey KB, Coffey BM, McCarthy E, Thomas W, and Jefferies CA (2013). Bruton's tyrosine kinase is required for apoptotic cell uptake via regulating the phosphorylation and localization of calreticulin. *J. Immunol* 190, 5207–5215. 10.4049/jimmunol.1300057. [PubMed: 23596312]
- Chang YY, and Neufeld TP (2009). An atg1/atg13 complex with multiple roles in TOR-mediated autophagy regulation. *Mol. Biol. Cell* 20, 2004–2014. 10.1091/mbc.e08-12-1250. [PubMed: 19225150]
- Deng H, Takashima S, Paul M, Guo M, and Hartenstein V (2018). Mitochondrial dynamics regulates *Drosophila* intestinal stem cell differentiation. *Cell Death Dis* 4, 81. 10.1038/s41420-018-0083-0.
- Derangère V, Chevriaux A, Courtaut F, Bruchard M, Berger H, Chalmin F, Causse SZ, LimagnE E, Végran F, Ladoire S, et al. (2014). Liver X receptor b activation induces pyroptosis of human and murine colon cancer cells. *Cell Death Differ* 21, 1914–1924. 10.1038/cdd.2014.117. [PubMed: 25124554]
- Dondelinger Y, Hulpiau P, Saeys Y, Bertrand MJM, and Vandenabeele P (2016). An evolutionary perspective on the necroptotic pathway. *Trends Cell Biol* 26, 721–732. 10.1016/j.tcb.2016.06.004. [PubMed: 27368376]
- Edenharter O, Schneuwly S, and Navarro JA (2018). Mitofusin-Dependent ER stress triggers glial dysfunction and nervous system degeneration in a *Drosophila* model of friedreich's ataxia. *Front. Mol. Neurosci* 11, 38. 10.3389/fnmol.2018.00038. [PubMed: 29563863]
- Freeman MR, Delrow J, Kim J, Johnson E, and Doe CQ (2003). Unwrapping glial biology: gcm target genes regulating glial development, diversification, and function. *Neuron* 38, 567–580. 10.1016/s0896-6273(03)00289-7. [PubMed: 12765609]
- Galluzzi L, Buqué A, Kepp O, Zitvogel L, and Kroemer G (2017). Immunogenic cell death in cancer and infectious disease. *Nat. Rev. Immunol* 17, 97–111. 10.1038/nri.2016.107. [PubMed: 27748397]
- Garg AD, and Agostinis P (2017). Cell death and immunity in cancer: from danger signals to mimicry of pathogen defense responses. *Immunol. Rev* 280, 126–148. 10.1111/imr.12574. [PubMed: 29027218]
- Goto S, and Hayashi S (1999). Proximal to distal cell communication in the *Drosophila* leg provides a basis for an intercalary mechanism of limb patterning. *Development* 126, 3407–3413. 10.1242/dev.126.15.3407. [PubMed: 10393119]
- Guo Z, and Ohlstein B (2015). Stem cell regulation. Bidirectional Notch signaling regulates *Drosophila* intestinal stem cell multipotency. *Science* 350, aab0988. 10.1126/science.aab0988. [PubMed: 26586765]
- Hetz C, and Mollereau B (2014). Disturbance of endoplasmic reticulum proteostasis in neurodegenerative diseases. *Nat. Rev. Neurosci* 15, 233–249. 10.1038/nrn3689. [PubMed: 24619348]
- Jewett KA, Thomas RE, Phan CQ, Lin B, Milstein G, Yu S, Bettcher LF, Neto FC, Djukovic D, Raftery D, et al. (2021). Glucocerebrosidase reduces the spread of protein aggregation in a *Drosophila melanogaster* model of neurodegeneration by regulating proteins trafficked by extracellular vesicles. *PLoS Genet* 17, e1008859. 10.1371/journal.pgen.1008859. [PubMed: 33539341]
- Katheder NS, Khezri R, O'Farrell F, Schultz SW, Jain A, Rahman MM, Schink KO, Theodossiou TA, Johansen T, Juhász G, et al. (2017). Micro-environmental autophagy promotes tumour growth. *Nature* 541, 417–420. 10.1038/nature20815. [PubMed: 28077876]
- Kirilly D, Spana EP, Perrimon N, Padgett RW, and Xie T (2005). BMP signaling is required for controlling somatic stem cell self-renewal in the *Drosophila* ovary. *Dev. Cell* 9, 651–662. 10.1016/j.devcel.2005.09.013. [PubMed: 16256740]

- Koehler CL, Perkins GA, Ellisman MH, and Jones DL (2017). Pink1 and Parkin regulate *Drosophila* intestinal stem cell proliferation during stress and aging. *J. Cell Biol* 216, 2315–2327. 10.1083/jcb.201610036. [PubMed: 28663346]
- Kuraishi T, Nakagawa Y, Nagaosa K, Hashimoto Y, Ishimoto T, Moki T, Fujita Y, Nakayama H, Dohmae N, Shiratsuchi A, et al. (2009). Pretaporter, a *Drosophila* protein serving as a ligand for Draper in the phagocytosis of apoptotic cells. *EMBO J* 28, 3868–3878. 10.1038/emboj.2009.343. [PubMed: 19927123]
- Lamkanfi M, Mueller JL, Vitari AC, Misaghi S, Fedorova A, Deshayes K, Lee WP, Hoffman HM, and Dixit VM (2009). Glyburide inhibits the Cryopyrin/Nalp3 inflammasome. *J. Cell Biol* 187, 61–70. 10.1083/jcb.200903124. [PubMed: 19805629]
- Lee T, and Luo L (1999). Mosaic analysis with a repressible cell marker for studies of gene function in neuronal morphogenesis. *Neuron* 22, 451–461. 10.1016/s0896-6273(00)80701-1. [PubMed: 10197526]
- Li W, and Baker NE (2007). Engulfment is required for cell competition. *Cell* 129, 1215–1225. 10.1016/j.cell.2007.03.054. [PubMed: 17574031]
- Lin L, Rodrigues FSLM, Kary C, Contet A, Logan M, Baxter RHG, Wood W, and Baehrecke EH (2017). Complement-related regulates autophagy in neighboring cells. *Cell* 170, 158–171.e8. 10.1016/j.cell.2017.06.018. [PubMed: 28666117]
- López-Otín C, Blasco MA, Partridge L, Serrano M, and Kroemer G (2013). The hallmarks of aging. *Cell* 153, 1194–1217. 10.1016/j.cell.2013.05.039. [PubMed: 23746838]
- Lu TY, MacDonald JM, Neukomm LJ, Sheehan AE, Bradshaw R, Logan MA, and Freeman MR (2017). Axon degeneration induces glial responses through Draper-TRAF4-JNK signalling. *Nat Commun* 8, 14355. [PubMed: 28165006]
- MacDonald JM, Beach MG, Porpiglia E, Sheehan AE, Watts RJ, and Freeman MR (2006). The *Drosophila* cell corpse engulfment receptor Draper mediates glial clearance of severed axons. *Neuron* 50, 869–881. 10.1016/j.neuron.2006.04.028. [PubMed: 16772169]
- Micchelli CA, and Perrimon N (2006). Evidence that stem cells reside in the adult *Drosophila* midgut epithelium. *Nature* 439, 475–479. 10.1038/nature04371. [PubMed: 16340959]
- Obeid M, Tesniere A, Ghiringhelli F, Fimia GM, Apetoh L, Perfettini JL, Castedo M, Mignot G, Panaretakis T, Casares N, et al. (2007). Calreticulin exposure dictates the immunogenicity of cancer cell death. *Nat. Med* 13, 54–61. 10.1038/nm1523. [PubMed: 17187072]
- Ohlstein B, and Spradling A (2006). The adult *Drosophila* posterior midgut is maintained by pluripotent stem cells. *Nature* 439, 470–474. 10.1038/nature04333. [PubMed: 16340960]
- Ohlstein B, and Spradling A (2007). Multipotent *Drosophila* intestinal stem cells specify daughter cell fates by differential Notch signaling. *Science* 315, 988–992. 10.1126/science.1136606. [PubMed: 17303754]
- Partridge L, Deelen J, and Slagboom PE (2018). Facing up to the global challenges of ageing. *Nature* 561, 45–56. [PubMed: 30185958]
- Patel PH, Dutta D, and Edgar BA (2015). Niche appropriation by *Drosophila* intestinal stem cell tumours. *Nat. Cell Biol* 17, 1182–1192. 10.1038/ncb3214. [PubMed: 26237646]
- Reiff T, Antonello ZA, Ballesta-Illán E, Mira L, Sala S, Navarro M, Martinez LM, and Dominguez M (2019). Notch and EGFR regulate apoptosis in progenitor cells to ensure gut homeostasis in *Drosophila*. *EMBO J* 38, e101346. 10.15252/emboj.2018101346. [PubMed: 31566767]
- Rivera Vargas T, and Apetoh L (2017). Danger signals: chemotherapy enhancers? *Immunol. Rev* 280, 175–193. 10.1111/imr.12581. [PubMed: 29027217]
- Rosado CJ, Mijaljica D, Hatzinisiriou I, Prescott M, and Devenish RJ (2008). Rosella: a fluorescent pH-biosensor for reporting vacuolar turnover of cytosol and organelles in yeast. *Autophagy* 4, 205–213. 10.4161/auto.5331. [PubMed: 18094608]
- Shinoda N, Hanawa N, Chihara T, Koto A, and Miura M (2019). Dronc-independent basal executioner caspase activity sustains *Drosophila* imaginal tissue growth. *Proc. Natl. Acad. Sci. U S A* 116, 20539–20544. 10.1073/pnas.1904647116. [PubMed: 31548372]
- Sim RB, Moestrup SK, Stuart GR, Lynch NJ, Lu J, Schwaeble WJ, and Malhotra R (1998). Interaction of CIq and the collectins with the potential receptors calreticulin (cClqR/Collectin receptor) and megalin. *Immunobiology* 199, 208–224. 10.1016/s0171-2985(98)80028-4. [PubMed: 9777407]

- Singh SR, Liu W, and Hou SX (2007). The adult *Drosophila* Malpighian Tubules are maintained by multipotent stem cells. *Cell Stem Cell* 1, 191–203. 10.1016/j.stem.2007.07.003. [PubMed: 18371350]
- Singh SR, Zeng X, Zhao J, Liu Y, Hou G, Liu H, and Hou SX (2016). The lipolysis pathway sustains normal and transformed stem cells in adult *Drosophila*. *Drosophila Nature* 538, 109–113. 10.1038/nature19788.
- Thomas RE, Vincow ES, Merrihew GE, MacCoss MJ, Davis MY, and Pallanck LJ (2018). Glucocerebrosidase deficiency promotes protein aggregation through dysregulation of extracellular vesicles. *PLoS Genet* 14, e1007694. 10.1371/journal.pgen.1007694. [PubMed: 30256786]
- Timmons AK, Mondragon AA, Schenkel CE, Yalonetskaya A, Taylor JD, Moynihan KE, Etchegaray JI, Meehan TL, and McCall K (2016). Phagocytosis genes nonautonomously promote developmental cell death in the *Drosophila* ovary. *Proc. Natl. Acad. Sci. U S A* 113, E1246–E1255. 10.1073/pnas.1522830113. [PubMed: 26884181]
- Tsuyama T, Kishikawa J.i., Han YW, Harada Y, Tsubouchi A, Noji H, Kakizuka A, Yokoyama K, Uemura T, and Imamura H (2013). In vivo fluorescent adenosine 5'-triphosphate (ATP) imaging of *Drosophila melanogaster* and *Caenorhabditis elegans* by using a genetically encoded fluorescent ATP biosensor optimized for low temperatures. *Anal. Chem* 85, 7889–7896. 10.1021/ac4015325. [PubMed: 23875533]
- Wallach D, Kang TB, Dillon CP, and Green DR (2016). Programmed necrosis in inflammation: toward identification of the effector molecules. *Science* 352, aaf2154. 10.1126/science.aaf2154. [PubMed: 27034377]
- Wang G, Xu J, Zhao J, Yin W, Liu D, Chen W, and Hou SX (2020). Arf1-mediated lipid metabolism sustains cancer cells and its ablation induces anti-tumor immune responses in mice. *Nat. Commun* 11, 220. 10.1038/s41467-019-14046-9. [PubMed: 31924786]
- Wang ZH, Clark C, and Geisbrecht ER (2016). *Drosophila* clueless is involved in Parkin-dependent mitophagy by promoting VCP-mediated Marf degradation. *Hum. Mol. Genet* 25, 1946–1964. 10.1093/hmg/ddw067. [PubMed: 26931463]
- Wang L, Zeng X, Ryoo HD, and Jasper H (2014). Integration of UPRER and oxidative stress signaling in the control of intestinal stem cell proliferation. *PLoS Genet* 10, e1004568. 10.1371/journal.pgen.1004568. [PubMed: 25166757]
- Wang S, Meyer H, Ochoa-Espinosa A, Buchwald U, Onel S, Altenhein B, Heinisch JJ, Affolter M, and Paululat A (2012). Gbf1 (gartenzwerg)-dependent secretion is required for *drosophila* tubulogenesis. *J. Cell Sci* 125, 461–472. 10.1242/jcs.092551. [PubMed: 22302994]
- Yuan J, Najafav A, and Py BF (2016). Roles of caspases in necrotic cell death. *Cell* 167, 1693–1704. 10.1016/j.cell.2016.11.047. [PubMed: 27984721]
- Zeng X, Chauhan C, and Hou SX (2010a). Characterization of midgut stem cell- and enteroblast-specific Gal4 lines in *Drosophila*. *Genesis* 48, 607–611. 10.1002/dvg.20661. [PubMed: 20681020]
- Zeng X, and Hou SX (2011). Kidney stem cells found in adult zebrafish. *Cell Stem Cell* 8, 247–249. 10.1016/j.stem.2011.02.008. [PubMed: 21362564]
- Zeng X, Singh SR, Hou D, and Hou SX (2010b). Tumor suppressors Sav/Scrib and oncogene Ras regulate stem cell transformation in adult *Drosophila* Malpighian Tubules. *J. Cell. Physiol* 224, 766–774. 10.1002/jcp.22179. [PubMed: 20432470]
- Zeng X, and Hou SX (2015). Enteroendocrine cells are generated from stem cells through a distinct progenitor in the adult *Drosophila* posterior midgut. *Development* 142, 644–653. 10.1242/dev.113357. [PubMed: 25670791]
- Zhou Z, Hartwig E, and Horvitz HR (2001). CED-1 is a transmembrane receptor that mediates cell corpse engulfment in *C. elegans*. *Cell* 104, 43–56. 10.1016/s0092-8674(01)00190-8. [PubMed: 11163239]

**Highlights**

- Knocking down Arf1 results in stem cell death through a sterile immunity-like pathway
- Knocking down Arf1 in intestinal stem cells induces expression of Prtp and Calr
- Prtp and Calr induce expression of Drpr and LRP1 in ECs via Mcr to produce ATP
- ATP kills ISCs by activating inflammasome-like pyroptosis

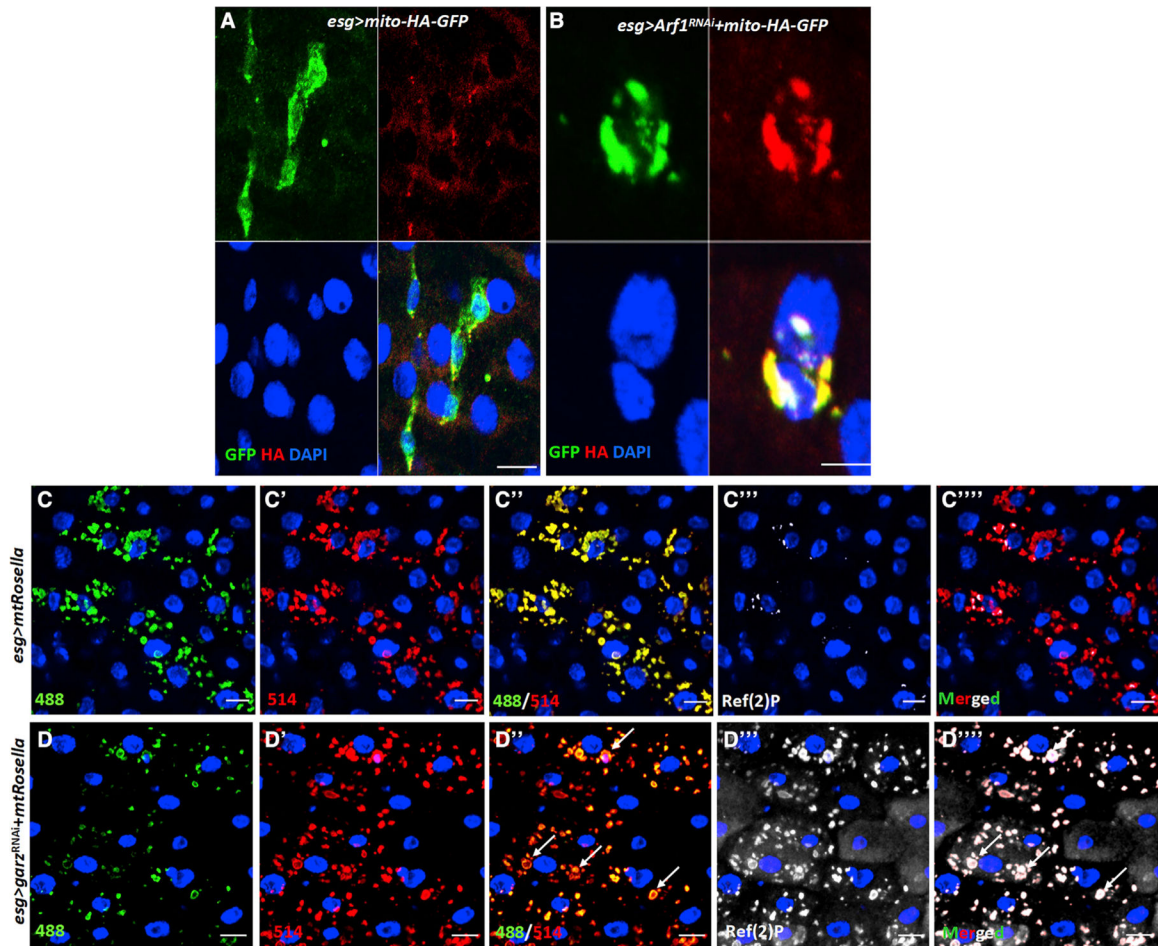


**Figure 1. Arf1 depletion in ISCs and EBs resulted in mitochondrial defects, mitophagy activation, and lysosomal protein aggregation**  
*esg<sup>ts</sup>>lacZ<sup>RNAi</sup>+mito-HA-GFP*, n = 35 (A); *esg<sup>ts</sup>>Arf1<sup>RNAi</sup>+mito-HA-GFP*, n = 31 (B);  
*esg<sup>ts</sup>>lacZ<sup>RNAi</sup>+mtRosella*, n = 33 (C–C'''''); *esg<sup>ts</sup>>garz<sup>RNAi</sup>+mtRosella*, n = 29 (D–D'''''). Flies with the indicated genotypes and treatments were cultured for 5 days at 29°C. Their midguts were dissected, stained with the indicated antibodies, and analyzed by confocal microscopy. White arrows point to colocalized red and white staining. n indicates the number of midguts examined for each genotype. Scale bars, 10 μm.

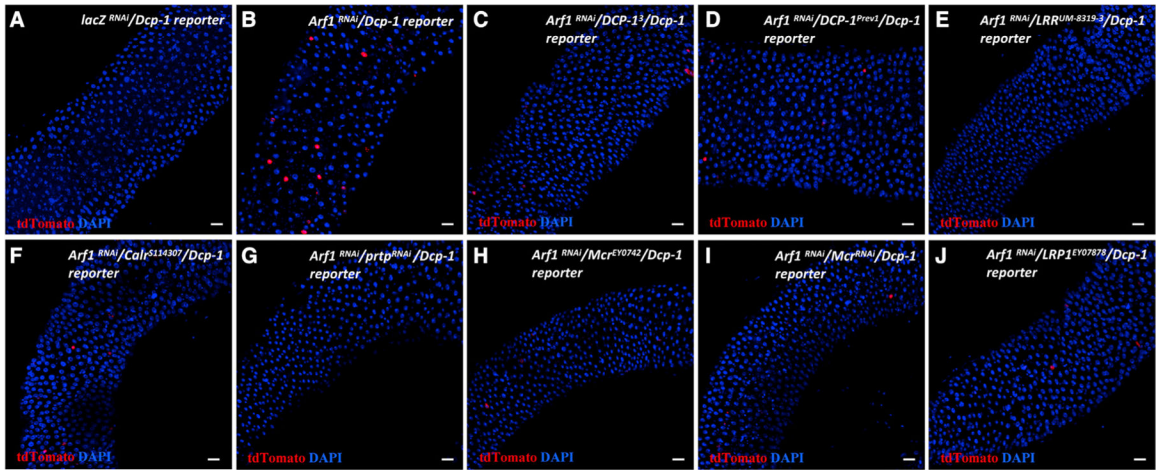


**Figure 2. New genes function downstream of Arf1 in regulating ISC survival**

The genotypes of the flies in each panel were as follows: (A) *lacZ*<sup>RNAi</sup>/*Dcp-1* reporter, n = 36; (B) *Arf1*<sup>RNAi</sup>/*Dcp-1* reporter, n = 32; (C) *Arf1*<sup>RNAi</sup>/*Dcp-1*<sup>3</sup>/*Dcp-1* reporter, n = 28; (D) *Arf1*<sup>RNAi</sup>/*Dcp-1*<sup>prev1</sup>/*Dcp-1* reporter, n = 33; (E) *Arf1*<sup>RNAi</sup>/*LRR*<sup>UM-8319-3</sup>/*Dcp-1* reporter, n = 26; (F) *Arf1*<sup>RNAi</sup>/*Calr*<sup>S114307</sup>/*Dcp-1* reporter, n = 29; (G) *Arf1*<sup>RNAi</sup>/*UAS-prtp*<sup>RNAi</sup>/*Dcp-1* reporter, n = 34; (H) *Arf1*<sup>RNAi</sup>/*Mcr*<sup>EY0742</sup>/*Dcp-1* reporter, n = 30; (I) *Arf1*<sup>RNAi</sup>/*Mcr*<sup>RNAi</sup>/*Dcp-1* reporter, n = 35; (J) *Arf1*<sup>RNAi</sup>/*LRP1*<sup>EY07878</sup>/*Dcp-1* reporter, n = 28. All RNAi was driven by *esg*<sup>ΔS</sup>. The *Dcp-1*-reporter was *Act-Dcp-1-QF*, *QUAS-tdTomato*. The posterior midgut of flies with the indicated genotypes was cultured for 4 days at 29°C, dissected, stained with the indicated antibodies, and analyzed by confocal microscopy. n indicates the number of midguts examined for each genotype. Scale bars, 10 μm.

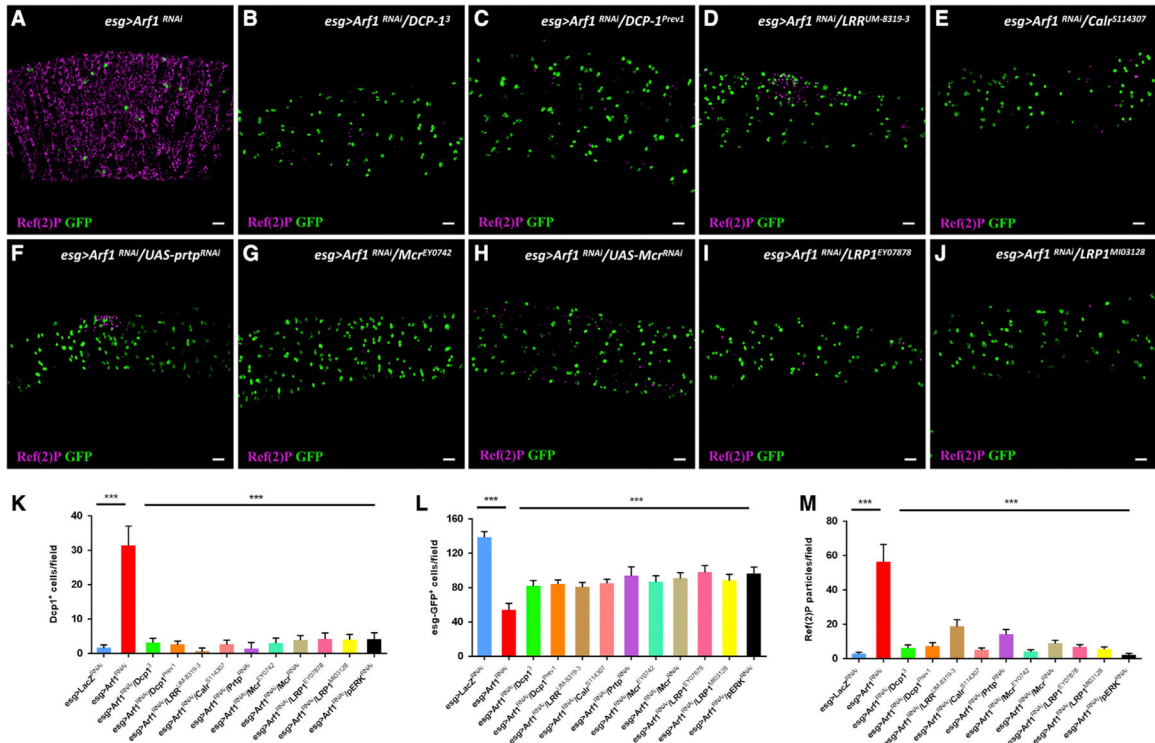


**Figure 3. New genes function downstream of Arf1 in regulating ISC survival**

(A–J) The genotypes of the flies in each panel were as follows: (A) *Arf1*<sup>RNAi</sup>, n = 37; (B) *Arf1*<sup>RNAi</sup>/*Dcp-1*<sup>3</sup>, n = 33; (C) *Arf1*<sup>RNAi</sup>/*Dcp-1*<sup>Prev1</sup>, n = 35; (D) *Arf1*<sup>RNAi</sup>/*LRR*<sup>UM-8319-3</sup>, n = 31; (E) *Arf1*<sup>RNAi</sup>/*Calr*<sup>S114307</sup>, n = 29; (F) *Arf1*<sup>RNAi</sup>/*prtp*<sup>RNAi</sup>, n = 34; (G) *Arf1*<sup>RNAi</sup>/*Mcr*<sup>EY0742</sup>, n = 31; (H) *Arf1*<sup>RNAi</sup>/*Mcr*<sup>RNAi</sup>, n = 36; (I) *Arf1*<sup>RNAi</sup>/*LRP1*<sup>EY07878</sup>, n = 29; (J) *Arf1*<sup>RNAi</sup>/*LRP1*<sup>MI03128</sup>, n = 32. All RNAi was driven by *esg*<sup>ts</sup>.

(K) Quantification of Dcp1<sup>+</sup> cells in the indicated panels.

(L) Quantification of GFP<sup>+</sup> cells in the indicated panels.

(M) Quantification of Ref(2)P<sup>+</sup> cells in the indicated panels.

The posterior midgut of flies with the indicated genotypes was cultured for 4 days at 29°C, dissected, stained with the indicated antibodies, and analyzed by confocal microscopy. Data show the mean ± SEM. Statistical significance was determined by Student’s t test; \*\*\*p < 0.001. n indicates the number of midguts examined for each genotype. Scale bars, 10 μm.

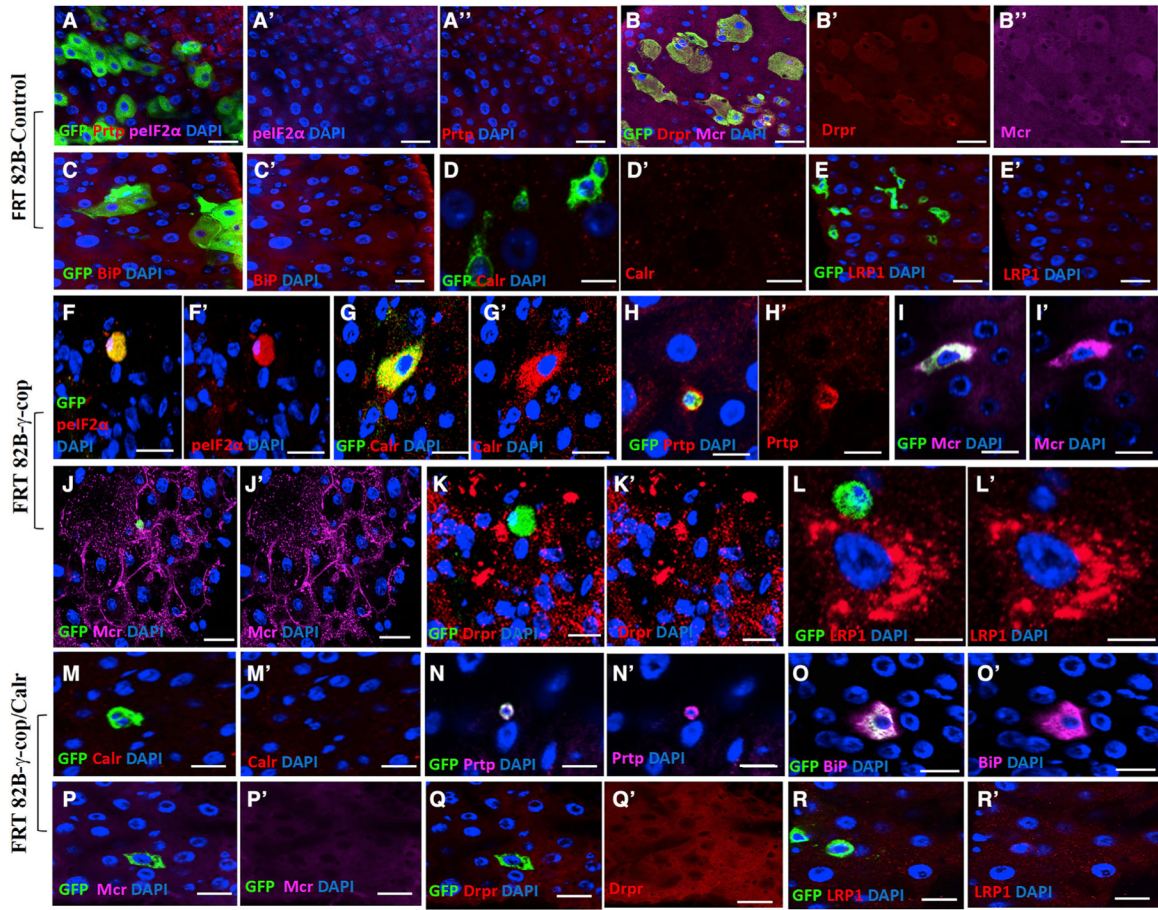


**Figure 4. Hierarchical relationship among Arf1 and new genes**  
 MARCM clones of flies with the following genotypes: (A–E') *FRT*<sup>82B</sup> control, n = 20; (F–L') *FRT*<sup>82B</sup>- $\gamma$ -*cop*<sup>10</sup>, n = 15; (M–R') *FRT*<sup>82B</sup>-*Calr*<sup>S062111</sup>- $\gamma$ -*cop*<sup>10</sup>, n = 17. The posterior midgut of flies with the indicated genotypes was dissected, stained with the indicated antibodies, and analyzed by confocal microscopy 3 days after clonal induction (ACI). n indicates the number of midguts examined for each genotype. Scale bars, 10  $\mu$ m.

**A**

	Drpr	Calr	LRP1	Mcr	Prtp
FRT <sup>82B</sup> -Control	-	-	-	-	-
FRT <sup>82B</sup> - $\gamma$ -cop <sup>10</sup>	+	+	+	+	+
FRT <sup>82B</sup> -Calr <sup>S062111</sup> , $\gamma$ -cop <sup>10</sup>	-	-	-	-	+
Prtp <sup><math>\Delta</math>1/+</sup> ; FRT <sup>82B</sup> - $\gamma$ -cop <sup>10</sup>	-	+	-	-	-
LRP1 <sup>M103128</sup> ; FRT <sup>82B</sup> - $\gamma$ -cop <sup>10</sup>	-	+	-	+/-	+
Mcr <sup>EY07421/+</sup> ; FRT <sup>82B</sup> - $\gamma$ -cop <sup>10</sup>	-	+	-		+
Dcp-1 <sup>3/+</sup> ; FRT <sup>82B</sup> - $\gamma$ -cop <sup>10</sup>	+	+	+	+	+

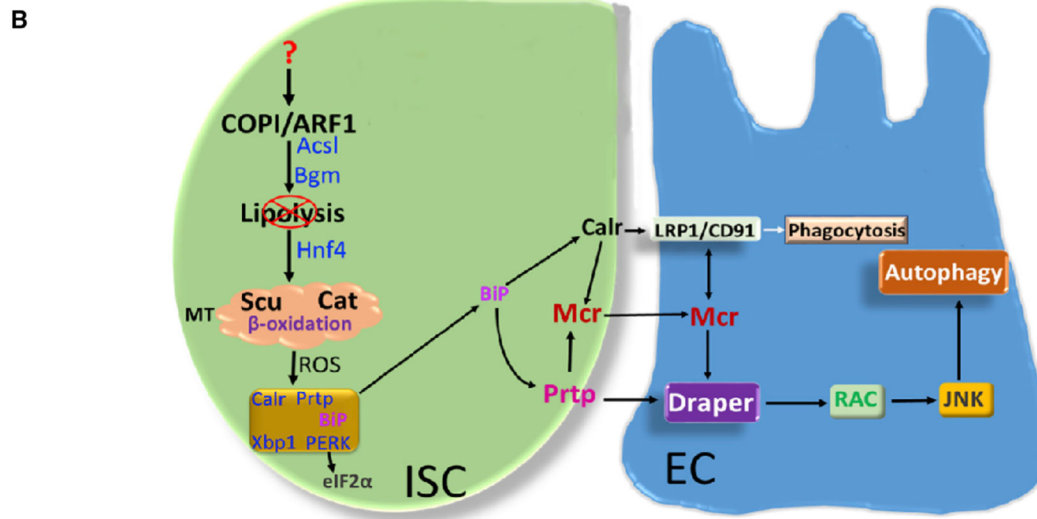


**Figure 5. Hierarchical relationship among Arf1 and new genes**

(A) We generated MARCM clones of *FRT<sup>82B</sup>- $\gamma$ -cop<sup>10</sup>* in different genetic backgrounds and examined the expression and localization of these proteins in the posterior midgut (original data are shown in Figures S3A–S3N). +, the protein was expressed; –, the protein was not expressed; +/-, the protein was weakly expressed.

(B) Model of coordinated ISC death induced by knockdown of the COPI/Arf1-lipolysis pathway.

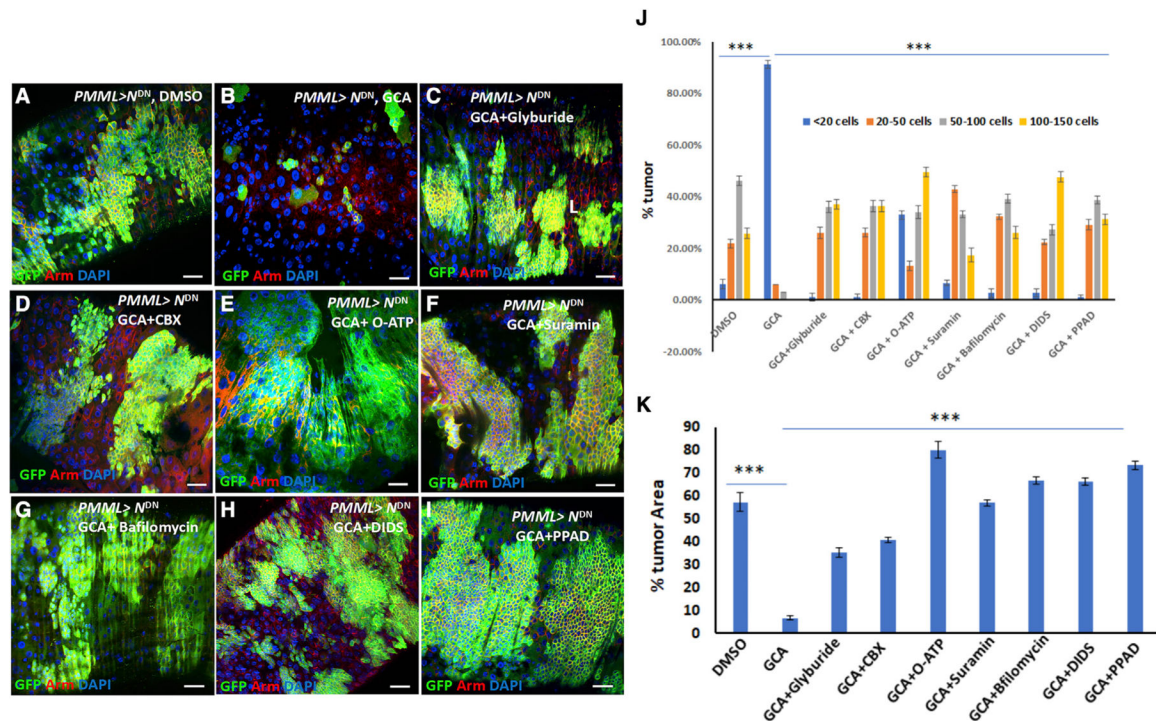


### Figure 6. Arf1 ablation kills stem cells through pyroptosis

(A–I) PMML clones of *FRT<sup>52B</sup>-UAS-Notch<sup>DN</sup>* were generated, and flies with *Notch<sup>DN</sup>*-tumors were given normal food containing DMSO (A), 5  $\mu$ M GCA (B), 5  $\mu$ M GCA + 40  $\mu$ M glyburide (C), 5  $\mu$ M GCA + 100  $\mu$ M CBX (D), 5  $\mu$ M GCA + 300  $\mu$ M O-ATP (Oxidized ATP) (E), 5  $\mu$ M GCA + 1 mg/mL suramin (F), 5  $\mu$ M GCA + 1  $\mu$ M Bafilomycin (G), 5  $\mu$ M GCA + 400  $\mu$ M DIDS (H), or 5  $\mu$ M GCA + 300  $\mu$ M PPAD (I).

(J) Quantification of tumor sizes in midgut in flies with the indicated treatments.

(K) Quantification of tumor areas in midgut in flies with the indicated treatments. We classify all tumors into four categories based on the total number of GFP positive cells in each tumor clone (<20 cells, 20–50 cells, 50–100 cells and 100–150 cells). Total numbers of tumors examined for each treatment: DMSO (132 tumors, n = 10 midguts), GCA (34 tumors, n = 10 midguts), GCA + Glyburide (89 tumors, n = 10 midguts), GCA + CBX (88 tumors, n = 10 midguts), GCA + O-ATP (91 tumors, n = 10 midguts), GCA + Suramin (121 tumors, n = 10 midguts), GCA + Bafilomycin (115 tumors, n = 10 midguts), GCA + DIDS (103 tumors, n = 10 midguts), or GCA + PPAD (103 tumors, n = 10 midguts).

Data show the mean  $\pm$  SEM. Statistical significance was determined by Student's t test, \*\*\*p < 0.001. Scale bars, 10  $\mu$ m.

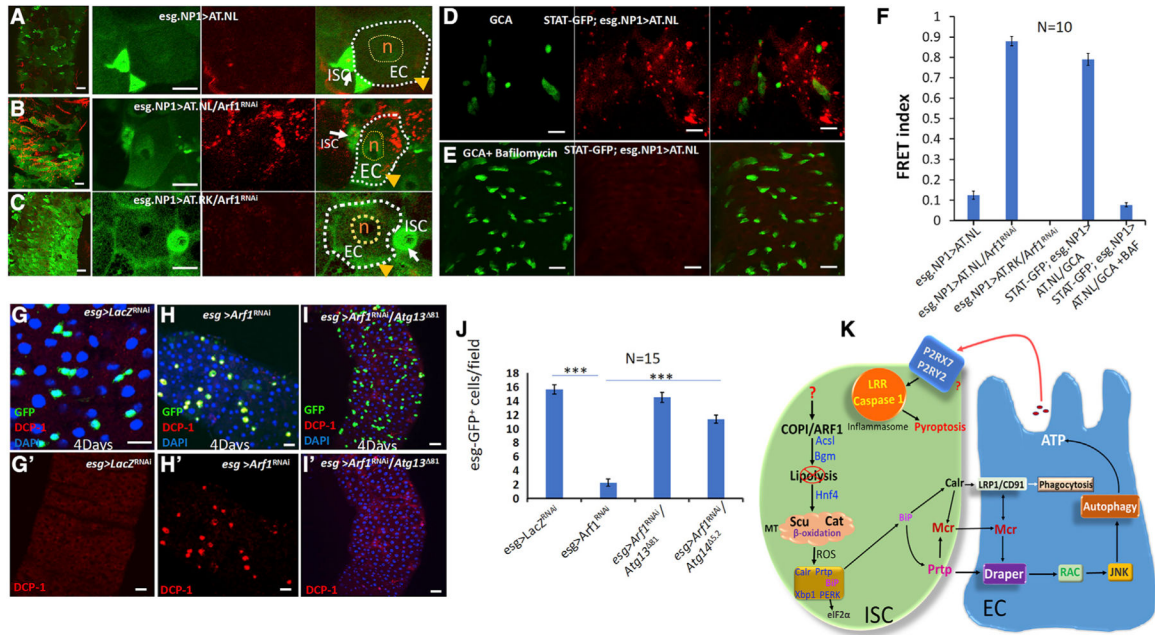


**Figure 7. Arf1 regulates ISC pyroptosis through ECs**

(A–C) Expression of an ATP reporter (*UAS-AT[NL]*) or its negative control (*UAS-AT[RK]*). *esg.NP1<sup>ts</sup>* is *esg-Gal4, NP1-Gal4;tub-Gal80<sup>S</sup>*, which drives gene expression in ISCs and ECs. Green, GFP from *esg.NP1<sup>ts</sup>>GFP*; red, ATP signal. (A) *esg.NP1<sup>ts</sup>>lacZ<sup>RNAi</sup> + AT[NL]*, n = 31. (B) *esg.NP1<sup>ts</sup>>Arf1<sup>RNAi</sup>+AT[NL]*, n = 33. (C) *esg.NP1<sup>ts</sup>>Arf1<sup>RNAi</sup>+AT[RK]*, n = 30.

(D and E) Signal Transducer and Activator of Transcription (STAT)-GFP; *esg.NP1<sup>ts</sup>* (-GFP)>*AT[NL]* flies were grown on food containing 5 μM GCA (D, n = 36) and 5 μM GCA + 1 μM Bafilomycin (E, n = 32). STAT-GFP (green) was used to mark ISCs and EBs, red shows the ATP signal.

(F) Quantitative measure of the fluorescence resonance energy transfer (FRET) signal in the indicated genotypes.

(G–I') Dcp-1 was induced in ISCs after Arf1 knockdown. (G and G') *esg<sup>ts</sup>>lacZ<sup>RNAi</sup>*. (H and H') *esg<sup>ts</sup>>Arf1<sup>RNAi</sup>*. (I and I') *esg<sup>ts</sup>>Arf1<sup>RNAi</sup>+Atg13<sup>81/+</sup>*.

(J) Quantification of *esg*+ cells with the indicated genotypes. 15 midguts were examined for each genotype (n = 15).

(K) Model of Arf1's regulation of ISC pyroptosis through ECs. The posterior midgut of flies with the indicated genotypes was cultured for 5 days at 29°C, dissected, stained with the indicated antibodies, and analyzed by confocal microscopy. Yellow arrows and white dotted lines indicate ECs, n indicates EC nuclei, and white arrow points to an ISC.

Data show the mean ± SEM. Statistical significance was determined by Student's t test, \*\*\*p < 0.001. n indicates the number of midguts examined for each genotype. Scale bars, 10 μm.

## KEY RESOURCES TABLE

REAGENT or RESOURCE	SOURCE	IDENTIFIER
<b>Antibodies</b>		
Anti-Draper 8A1 Antibody (mouse)	Developmental Studies Hybridoma Bank	Cat# Draper 8A1; RRID: AB_2618106
Anti-N2 7A1 Armadillo Antibody (mouse)	Developmental Studies Hybridoma Bank	Cat# N2 7A1 ARMADILLO; RRID: AB_528089
Anti-LRP1 Antibody (rabbit)	Kind gift from Prof. S. Eaton	N/A
Anti-Mcr Antibody (guinea pig)	Kind gift from Dr. R. Ward	N/A
Anti-Calreticulin Antibody (rabbit)	Abcam	Cat# ab2907; RRID: AB_303402
Anti-Prtp Antibody (mouse)	This manuscript	N/A
Anti-Grp78/HSPA5 (rabbit)	Novus Biologicals	Cat# NBP1-06274; RRID: AB_1555284
Anti-Phospho-eIF2 $\alpha$ (Ser51) Antibody (rabbit)	Cell Signaling Technology	Cat# 9721; RRID: AB_330951
Anti-Ref2P antibody	Abcam	Cat # ab178440
Anti-HA tag antibody	Abcam	Cat# ab9110; RRID: AB_307019
anti-GFP Antibody (rabbit)	Thermo Fischer Scientific	Cat# A-6455; RRID: AB_221570
anti-GFP Antibody (rabbit)	Thermo Fischer Scientific	Cat# A-11120; RRID: AB_221568
Anti-DCP1 Antibody (rabbit)	Cell Signaling Technology	Cat# 9578; RRID: AB_2721060
Goat anti-rabbit Alexa Fluor 488	Thermo Fischer Scientific	Cat# A-11008; RRID: AB_143165
Goat anti-rabbit Alexa Fluor 568	Thermo Fischer Scientific	Cat# A-11011; RRID: AB_143157
Goat anti-rabbit Alexa Fluor 633	Thermo Fischer Scientific	Cat# A32733; RRID: AB_2633282
Goat anti-mouse Alexa Fluor 488	Thermo Fischer Scientific	Cat# A-11001; RRID: AB_2534069
Goat anti-mouse Alexa Fluor 568	Thermo Fischer Scientific	Cat# A-11004; RRID: AB_2534072
Goat anti-guinea pig Alexa Fluor 568	Thermo Fischer Scientific	Cat# A-11075; RRID: AB_141954
<b>Chemicals, peptides, and recombinant proteins</b>		
Sodium 4-Phenylbutyrate (PBA)	Merck Millipore	Cat # 567616
GSK2606414	Merck Millipore	Cat # 516535
Golgicide A (GCA)	Cayman Chemical	Cat # 18430
Glyburide	Cayman Chemical	Cat # 15009
Carbenoxolone (CBX) disodium salt	Sigma-Aldrich	Cat # C4790
Adenosine 5'-triphosphate, periodate oxidized sodium salt (oxATP)	Sigma-Aldrich	Cat # A6779
Bafilomycin A1	Sigma-Aldrich	Cat # B1793
Suramin	Sigma-Aldrich	Cat # S2671
DIDS (Sodium salt)	Cayman Chemical	Cat # 16125
PPAD (Sodium salt)	Cayman Chemical	Cat # 14537
DMSO	Sigma-Aldrich	Cat # 276855
Vectashield + DAPI	Vector Laboratories	Cat # H1200
Paraformaldehyde	Electron Microscopy Science	Cat # 15710
<b>Experimental models: Organisms/strains</b>		
Y[1] sc[*] v[1]; UAS-prtp <sup>RNAi</sup>	Bloomington Drosophila Stock Center	56965
Y[1] sc[*] v[1]; UAS-LRR <sup>RNAi</sup>	Bloomington Drosophila Stock Center	41686
UAS-LRR <sup>RNAi</sup>	National Institute of Genetics	1399R-1

REAGENT or RESOURCE	SOURCE	IDENTIFIER
W1118; P{RS3}LRR <sup>UM-8319-3</sup>	Kyoto Stock Center	124478
Y[1] sc[*] v[1]; UAS-Dcp1 <sup>RNAi</sup>	Bloomington Drosophila Stock Center	38315
Y[1] w[*]; Dcp-1 <sup>Prev1</sup>	Bloomington Drosophila Stock Center	63814
Y[1] w[*]; Dcp-1 <sup>3</sup>	Bloomington Drosophila Stock Center	63815
Y[1] sc[*] v[1]; UAS-PEK <sup>RNAi</sup>	Bloomington Drosophila Stock Center	35162
Yw[1118], ey-FLP; neoFRT <sup>82B</sup> , Calr <sup>S062111</sup> /TM3,Ser	Bloomington Drosophila Stock Center	37724
Y[1] w[67c23]; Calr <sup>S114307</sup> /TM3,Sb, Ser	Bloomington Drosophila Stock Center	4545
UAS-Mcr <sup>RNAi</sup>	Vienna Drosophila Resource Center	KK100197
Y[1] sc[*] v[1]; UAS-Mcr <sup>RNAi</sup>	Bloomington Drosophila Stock Center	65896
Y[1] w[67c23];Mcr <sup>EY07421</sup> /Cy0	Bloomington Drosophila Stock Center	15997
Drpr <sup>5</sup>	Freeman et al. 2003	N/A
UAS-BiP <sup>RNAi</sup>	Bloomington Drosophila Stock Center	32402
prtp <sup>1</sup>	Kuraishi et al. 2009	WA
prtp <sup>2</sup>	Kuraishi et al. 2009	N/A
UAS-AT1.NL	Tsuyama et al. 2013	N/A
UAS-AT1.RK	Tsuyama et al. 2013	N/A
UAS-mtRoseella	Edenharter et al., 2018	WA
esg-Gal4	Goto and Hayashi., 1999	N/A
NP1-Gal4	Kyoto Stock Center	112001
UAS-Arf1 <sup>RNAi</sup>	Vienna Drosophila Resource Center	103572
UAS-Arf1 <sup>RNAi</sup>	Vienna Drosophila Resource Center	23080
UAS-garz <sup>RNAi</sup>	Vienna Drosophila Resource Center	42140
UAS-Acs1 <sup>RNAi</sup>	Bloomington Drosophila Stock Center	27729
P{w[+mC] = UAS-mito-HA-GFP.AP}/Cy0	Bloomington Drosophila Stock Center	8442
pmCherry-Atg8a	Kind gift from Dr. Gabor Juhasz	WA
Atg13 <sup>81</sup>	Chang and Neufeld, 2009	WA
Atg14 <sup>5.2</sup>	Katheder et al., 2017	N/A
Y[1] w[67c23]; LRP1 <sup>EY07818</sup>	Bloomington Drosophila Stock Center	16864
garz <sup>211</sup>	Wang et al. 2012	N/A
Y[1] w[*]; LRP1 <sup>Mi03128</sup>	Bloomington Drosophila Stock Center	58610
Y[1] v[1]; UAS-Xbp1 <sup>RNAi-1</sup>	Bloomington Drosophila Stock Center	25990
Y[1] v[1]; UAS-Xbp1 <sup>RNAi-2</sup>	Bloomington Drosophila Stock Center	36755
FRT <sup>82B</sup> -γ-COP <sup>10</sup>	Bloomington Drosophila Stock Center	29703
<b>Software and algorithms</b>		
Zen	Carl Zeiss	<a href="https://zeiss.com/">https://zeiss.com/</a>
Prism 8.1.2	GraphPad	<a href="https://www.graphpad.com/">https://www.graphpad.com/</a>
ImageJ	NIH	<a href="https://imagebni.gov/Windex.html">https://imagebni.gov/Windex.html</a>
Photoshop 2021	Adobe	<a href="https://www.adobe.com/cy_en/products/photoshop.html">https://www.adobe.com/cy_en/products/photoshop.html</a>